Radiocarbon ($\Delta^{14}C$) and stable carbon ($\delta^{13}C$) isotopic composition of dissolved inorganic carbon (DIC) in Baffin Bay

Student: Sara Zeidan
Supervisor: Dr. Brett Walker

In partial fulfillment of the requirements for the M.Sc. degree in Earth Sciences

uOttawa

Abstract

It has been estimated that approximately half of all anthropogenic fossil fuel carbon dioxide (CO_2) emissions have been absorbed by the oceans. Air-sea gas exchange of CO_2 and the buffering capacity of seawater allows the oceans to store significant amounts of dissolved inorganic carbon (DIC; ~38,000 GtC). The Arctic Ocean is currently warming at double the rate of the rest of the planet, yet the effect of climate change on the Arctic marine carbon cycle remains unconstrained. Recent work suggests that Arctic marine environments are a carbon sink for the majority of the year, and plays a key role in storing anthropogenic carbon below the mixed layer. Baffin Bay is a semi-enclosed, Arctic basin that supplies cold surface water to the Labrador Sea; a critical region for North Atlantic deep-water formation. While the physical oceanography of surface Baffin Bay is well characterized, less is known about deep water formation mechanisms and its ventilation age. The few residence times for Baffin Bay Deep Water (BBDW) range widely from 20-1450 years. Improved residence time estimates are essential for understanding the role Baffin Bay plays in the Arctic carbon cycle and how this region will respond to climate change. Radiocarbon ($\Delta^{14}C$) and stable carbon ($\delta^{13}C$) measurements of DIC are powerful tools for parameterizing water mass sources, aging and residence times. However, very few DIC $\Delta^{14}C$ and $\delta^{13}C$ data have been reported in the Arctic Ocean, comprising only a handful of stations in the Eurasian Basin, Canadian Basin, and Beaufort Sea.

With this goal in mind, we conducted a study in which DIC samples were collected aboard the CCGS *Amundsen* in 2019 for $\delta^{13}C$ and $\Delta^{14}C$ analysis. DIC $\delta^{13}C$ and $\Delta^{14}C$ values ranged from 0.68‰ to +1.90‰ and -90.0‰ to +29.8‰, respectively. Surface DIC $\delta^{13}C$ values were +0.69‰ to +1.90‰, while deep (>100m) $\delta^{13}C$ values ranged -0.01 to -0.68‰. Significant linear correlations were found for $\delta^{13}C$ and potential density, suggesting DIC $\delta^{13}C$ is an effective water mass and carbon source tracer in Baffin Bay. Surface DIC $\Delta^{14}C$ values ranged -5.4‰ to +22.9‰, while deep DIC (>1400m) DIC $\Delta^{14}C$ averaged -82.2±8.5‰ (n = 9). Much larger surface to deep gradients in DIC $\Delta^{14}C$ are observed in Baffin Bay vs. that of the North Atlantic Ocean, suggesting significant aging of BBDW. Next, we used the potential alkalinity method (P_{alk}) and the ΔC^* method to quantify the amount of "bomb" ^{14}C and anthropogenic C (DIC_{anth}) to model "natural" DIC $\Delta^{14}C$ profiles. Both P_{alk} and ΔC^* proxies had high errors in cold, low salinity surface water. In particular, surface (<400m) $\Delta^{14}C_{bomb}$ was overestimated at all stations. However, both proxies did not indicate $\Delta^{14}C_{bomb}$ or DIC_{anth} contributions below 1000m. Two ^{14}C residence times were

estimated based on two proposed mechanisms of BBDW formation. A residence time of 690 ±35 years was estimated assuming surface brine rejection in Nares Strait is the main source of BBDW. Another plausible source of BBDW is the entrainment of dense north Atlantic Water over Davis Strait mixed with brine enriched surface water. A comparison of DIC_{anth} and $\Delta^{14}C_{bomb}$ corrected deep DIC $\Delta^{14}C$ values from the North Atlantic (GO-SHIP A16N) to BBDW, resulted in a residence time of 360 ±35 years. These residence times (360-690 years) provide new constraints on the ventilation age of deep Baffin Bay and suggest this basin has the potential to store carbon for centuries.

Acknowledgments

The completion of this thesis could not have been possible without the assistance and support of many colleagues, collaborators, family, and friends. Their contributions are greatly appreciated and acknowledged.

I would like to thank my supervisor, Dr. Brett Walker, for his utmost and continuous support over the course of my graduate degree. His guidance, patience, and motivation have made the completion of my thesis both enjoyable and memorable. Dr. Walker's expertise and guidance have taught me important skills in scientific research, that of which I will carry on throughout the rest of my career. Above all, I would like to thank Dr. Walker for his kindness and friendship, and I am extremely grateful for the opportunities he has provided me with. I would also like to thank his wife, Jennifer Walker, for all her help throughout the years. The completion of this research project would not have been possible without her support and expertise.

I would also like to thank Chief Scientist Alexandre Forest, Anissa Merzouk, the staff of Amundsen Science, and the crew of the CCGS *Amundsen* for the opportunity and coordination to participate in the 2019 research expedition in Baffin Bay. I am also grateful to Dr. Cara Manning for coordinating sampling and logistics on the cruise, as well as Tonya Brugers (University of Manitoba) and Shawn Marriott (University of Calgary) for DIC and A_T sample collection and analysis. I would also like to thank members of the UC Irvine Keck Carbon Cycle AMS lab, Dr. Xioamei Xu and Di John Southon, for ^{14}C analysis of my graphite samples. As well, I would like to thank members of the Ján Veizer Stable Isotope Laboratory, Paul Middlestead and his staff, for $\delta^{13}C$ analysis of my seawater samples.

Finally, I would like to thank my parents for their endless love, support, and sacrifices they have made for my education and future. I am also extremely thankful to my friends and family who have always supported and motivated me to complete my research. Without their unconditional love and care, none of this would have been possible.

List of Figures

Figure 1, Page 25 – Sample locations, gateways and currents of Baffin Bay

Figure 2, Page 26 – Depth profiles of DIC $\delta^{13}C$ and $\Delta^{14}C$ values in Baffin Bay.

Figure 3, Page 27 – Potential temperature-salinity diagram with DIC $\delta^{13}C$ values throughout Baffin Bay

Figure 4, Page 28 – Calculated $\Delta^{14}C_{bomb}$ and $\Delta^{14}C_{natural}$ values for Baffin Bay deep water.

Figure 5, Page 29 – Calculated DIC_{anth} concentrations found throughout central and Eastern Baffin

Figure 6, Page 30– Calculated apparent $\Delta^{14}C$ age based on correct $\Delta^{14}C$ values for BB2 and A16N stations

Figure B1, Page 50 - Regressions of potential density versus DIC $\delta^{13}C$ for Baffin Bay stations. Lines are Least squares fit linear regression. Line equations and coefficients of determination (R^2) values are listed next to the trendline.

Figure B2 Page 51 - Regressions of potential density versus DIC $\Delta^{14}C$ for Baffin Bay stations. Lines are Least squares fit linear regression. Line equations and coefficients of determination (R^2) values are listed next to the trendline.

Figure B3, Page 52 - Regressions of potential density versus DIC $\delta^{13}C$ for distinct regions in Baffin Bay; Northern Gateway stations consist of 108 and 323, Central Baffin Bay stations consist of 193, BB2, and 224, and West Greenland stations consist of 196, BB15, BB18, 227, 204, and 210. Lines are Least squares fit linear regression. Line equations and coefficients of determination (R^2) values are listed next to the trendline.

Figure B4 Page 53 - Regressions of salinity versus DIC $\delta^{13}C$ for Baffin Bay stations for surface, mid-depth and deep sample data. Depth-specific regressions are shown for; surface (0 – 100m), mid-depth (100 – 800m), and deep (>800m). Lines are Least squares fit linear regression. Line equations and coefficients of determination (R^2) values are listed next to each trendline.

List of Tables

Table A1, Page 41- Summary of measured data from the CCGS Amundsen in July 2019 in Baffin Bay

Table A2, Page 44 - Modeled anthropogenic carbon (C_{anth}) concentrations calculated from the ΔC^* proxy based on calculations presented by Lee et al., (2003). Bomb $\Delta^{14}C$ and Natural (measured – bomb) $\Delta^{14}C$ signatures presented calculated from the potential alkalinity (Palk) method presented by Rubin and Key., (2002).

Table B1, Page 47 - Potential density (kg m^{-3}) versus DIC $\delta^{13}C$ (‰) least squares linear regression statistics for slope coefficients, y-intercepts, coefficients of determination (R^2) and p-values.

Table B2, Page 48 - Potential density (kg m^{-3}) versus DIC $\Delta^{14}C$ (‰) least squares linear regression statistics for slope coefficients, y-intercepts, coefficients of determination (R^2) and p-values.

Table B3, Page 49 - Salinity versus DIC $\delta^{13}C$ (‰) least squares linear regression statistics for slope coefficients, y-intercepts, coefficients of determination (R^2) and p-values.

Table of Contents

Abstract ii
Acknowledgments iv
List of Figures v
List of Tables vi
1. Literature Review 1
1.1 Baffin Bay Surface Currents and Hydrographic Setting 1
1.2 Baffin Bay Volume Transport 2
1.3 Baffin Bay Water Masses 3
1.4 DIC $\Delta^{14}C$ and $\delta^{13}C$ Isotopic Composition of the Arctic Ocean 4
2. Introduction 7
3. Methods 9
3.1 Sample collection 9
3.2 DIC, Total Alkalinity, salinity, and nutrient analysis 9
3.3 Stable isotope ($\delta^{13}C$) analysis 10
3.4 Natural abundance radiocarbon ($\Delta^{14}C$) analysis 10
3.5 Estimation of anthropogenic (DIC_{anth}) and "bomb" DIC ^{14}C 11
4. Results 13
4.1 DIC $\delta^{13}C$ values 13
4.2 DIC $\Delta^{14}C$ values 13
5. Discussion 14
5.1 Baffin Bay – hydrographic setting 14
5.2 DIC $\delta^{13}C$ as a water mass tracer 15
5.3 DIC $\Delta^{14}C$ distributions in Baffin Bay 17
5.4 Estimation of DIC $\Delta^{14}C_{bomb}$ contributions 19
5.5 Estimating anthropogenic DIC contributions 20
5.6 Estimating a ^{14}C-based residence age estimates for deep Baffin Bay 21
6. Summary and Implications 23
7. Acknowledgments 23
8. Data availability 24
9. Figures and Captions 25
10. Conclusion 31
11. References 33
Appendix A: Extended data tables of measured and derived parameters 41
Appendix B: DIC $\delta^{13}C$ and $\Delta^{14}C$ least squares regression analysis and statistics summary 47

1. Literature Review

1.1 Baffin Bay Surface Currents and Hydrographic Setting

Two major surface currents govern Baffin Bay (Figure 1); the West Greenland Current (WGC) and the Baffin Island Current (BIC). The WGC enters Baffin Bay through the Davis Strait, bringing warm salty Atlantic water along the East coast of Baffin Bay as it travels northward (Bourke et al., 1989). The subsurface WGC is found at around 500 m along the East coast of Baffin Bay, characterized by temperature of ~2.0 °C, a salinity of 34.5, and a density of 27.6 kg/m^3 (Münchow et al., 2015) The WGC has two southerly components; a fresher component which travels along the shallow Greenland shelf originating from Fram Strait, and a warmer saltier component known as the West Greenland Slope Current (WGSC), which travels along the slope of Greenland from the North Atlantic (Curry et al., 2011). As the WGC travels northward, it becomes modified through glacial and sea-ice melt and progressively cools and freshens (Myers et al., 2009). The BIC enters Baffin Bay through two northern Arctic gateways, transporting cold, fresh water along the East coast of Baffin Island. The BIC exits Baffin Bay over the Davis Strait where it enters the North Atlantic Ocean (Fissel et al., 1982). The BIC is characterized by waters that are below -1.6°C, a salinity of less than 33.8 psu, and density of less than 27.6 kg/m^3 (Münchow et al., 2015).The combination of the northward WGC and southward BIC forms a cyclonic gyre along the surface waters of Baffin Bay (Figure 1).

The WGC consists of both Atlantic and Arctic origin. Arctic waters from the Eurasian Basin exit along the East coast of Greenland through Fram Strait. These waters flow southward along the Eastern coast of Greenland as the East Greenland Current (EGC), eventually reaching the Southern tip of Greenland and entering Baffin Bay as the WCG (Curry et al., 2014). As the EGC travels along the coast of Greenland, it becomes modified through coastal inflow and glacial runoff (Bacon et al., 2002). The Irminger Current combines with the EGC and enters Baffin Bay through the Eastern Davis Strait to form the WGC. This warmer, saline WGC current remains offshore of Western Greenland, and helps keep the coast of Greenland ice free (Sutherland and Pickart, 2008). The BIC contains both Arctic and Pacific water. Cool fresh Arctic Waters from the Lincoln Sea and Canadian Arctic Archipelago (CAA) enter Baffin Bay through the Northern gateways (Nares Strait and Lancaster Sound, respectively) and combine to form the surface BIC

(Cuny et al., 2005). The BIC also contains some remnants of the WGC modified by local sea ice formation and melt (Azetsu-Scott et al., 2012).

1.2 Baffin Bay Volume Transport

The CAA exports around half of the freshwater from the Arctic into the Northern Atlantic Ocean through Baffin Bay (Serreze et al., 2006). Arctic water travelling into Baffin Bay consists of three primary freshwater sources: meteoric water, sea ice meltwater, and Pacific Water. The Pacific Ocean contains meteoric water from rivers and precipitation. One third of the freshwater in the Arctic Ocean is provided via the Pacific Ocean, transported through the Bering Strait, CAA and subsequently into Baffin Bay (Alkire et al., 2010). Another large source of freshwater input in Baffin Bay is runoff from the Greenland ice sheet. Increasing meltwater runoff into both in Baffin Bay and the North Atlantic Ocean has been observed due to climate change. For example, meltwater from the Greenland ice sheet is found in the top 30 m of the water column in Baffin Bay, usually as glacial melt and icebergs (Tang et al., 2004). The loss of the Greenland ice sheet is accelerating at a rate of 22±1 Gt/yr^2 based on data from 1992 to 2010 (Rignot et al., 2011). In 2019, Greenland saw the most ice loss (532 Gt) in any year since 1948 (Sasgen et al., 2020). Roughly 80% of discharge from the ice sheet is located west and south-east of Greenland, with 22% of this portion entering Baffin Bay (Bamber et al., 2012).

Mean volume transport has been calculated for each of the major north gateways into Baffin Bay: 1) Barrow Strait is estimated at 0.46 ± 0.09 Sv (Peterson & Pettipas., 2013), 2) Strait-Hell Gate located North of Jones Sound is estimated to be 0.3 Sv (Melling et al., 2008) and 3) Nares Strait is estimated to be 0.57 ± 0.09 Sv (Münchow and Melling, 2008). There is a total mean volume transport of ~1.5 Sv through the CAA into Baffin Bay. A total mean freshwater transport of 0.1 Sv has also been reported (Hamilton and Wu, 2013). As mentioned above, the BIC and WGC transport water out of and into Baffin Bay over the Davis Strait. Based on mooring meridional velocity data, this mean annual volume transport is 1.2 ± 0.7 Sv northward across David Strait, and 4.6±1.1Sv southward (Cuny et al., 2005). Of this, 22 ± 17 mSv (1 mSv = 10^3 m^3/s) is northward and 152 ± 58 mSv is southward freshwater transport (Cuny et al., 2005). Significant amounts of sea-ice (528 km^3) are also transported through the Davis Strait annually (Cuny et al., 2005).

1.3 Baffin Bay Water Masses

Subsurface Baffin Bay contains several distinct water masses. The Halocline layer (HL; salinity = 32.80- 34.20, σ_θ ~27.04 kg/m^3) extends from ~30 to 300m (Lehmann et al., 2019). The HL incapsulates two distinct water masses; the Arctic Water (AW) and the West Greenland Shelf Water (WGSW). AW (2°C, salinity = 33.70) can be further modified by glacial run off and local sea ice melt as it travels with the BIC (Curry et al., 2014). The WGSW (< 7°C, salinity < 34.1) is an extension of the EGC (Curry et al., 2014). Intermediate Water (IW; >0.4°C, salinity >34.20, σ_θ ~27.6 kg/m^3) is found between 300 – 1200m (Lehmann et al., 2019). The West Greenland Irminger Water (WGIW; >2°C, salinity >34.1) is the main component of IW in Baffin Bay and is North Atlantic water from the Irminger Sea which enters Eastern Baffin Bay through Davis Strait as a barotropic current (Curry et al., 2014). As WGIW travels northward, it cools and freshens due to both vertical and lateral mixing. A portion of the IW enters Lancaster and Smith Sounds as it circulates in Baffin Bay. However, the majority of IW eventually flows southward, beneath the surface BIC (Bourke et al., 1989). Transitional Water (TrW; ≤2°C, salinity >33.7) is also an IW component, representing a combination of AW and IW modified through processes such as mixing and brine rejection (Curry et al., 2014).

Baffin Bay Deep Water (BBDW; 0°C, salinity <34.5, σ_θ ~27.69 kg/m^3) can be found between 1200 to 1800m. Below 1800m, is Baffin Bay Bottom Water (BBBW; -0.4°C, salinity ~35.4, and σ_θ = 27.72 kg/m^3; Lehmann et al., 2019). Since the Davis Strait has a sill depth of 640m, there is no direct exchange of BBDW and BBBW with the Arctic or Atlantic Oceans. Deep water formation of BBBW is still a matter of scientific debate (Tang et al., 2004). Some have suggested that cold, salty waters are produced in the winter during enhanced freezing in thin ice and open water of the North Water near Smith Sound (Bourke et al., 1989). Other studies suggest that deep and bottom waters contain waters of similar properties to those found at 250m depth in the Beaufort Sea (Bailey, 1956). Halocline water of the Barents Sea also contain similar properties, which can be found near Nares Strait (Rudels et al., 2004). Both these theories suggest that the Arctic Ocean is a primary source of both deep and bottom waters of Baffin Bay. Another potential source of Baffin Bay deep water is the input of dense Labrador seawater over Davis Strait, which mix with brine rejected surface waters during the winter months (Murphy et al., 1944). The residence time of BBBW is understudied. To date, only 3 residence time estimates exist; i) 20 years based on volume transport estimates (Sadler, 1976), ii) 77 years based on ^{3}He/Tritium data using a box

model approach (Top et al., 1980) and iii) 1,450 years based on a chlorofluorocarbon (CFC) tracer box model (Wallace, 1985).

1.4 DIC $\Delta^{14}C$ and $\delta^{13}C$ Isotopic Composition of the Arctic Ocean

Radiocarbon ($\Delta^{14}C$) and stable carbon ($\delta^{13}C$) isotopes are powerful tools for quantifying chemical, biological, and physical oceanographic processes. Atmospheric nuclear weapon testing took place in the 1950s and 1960s and released 6 x 10^{28} ^{14}C atoms into the global atmosphere (Naegler and Levin, 2006). The incorporation of bomb ^{14}C into the global oceans DIC reservoir has provided a useful oceanographic tracer of air-sea gas exchange and surface currents (Brown and Reimer, 2004). Similarly, the fossil fuel CO_2 emissions have impacted Earth's atmosphere (i.e. The Suess Effect) with isotopically heavy $\delta^{13}C$ and ^{14}C-free CO_2 (Suess 1953). Thus, DIC $\delta^{13}C$ and $\Delta^{14}C$ can be used to estimate both the relative contributions of anthropogenic (fossil) vs. bomb carbon and also as a "clock" of water mass aging with radioactive decay. DIC $\Delta^{14}C$ distributions can therefore provides estimates of deep water circulation and aging.

Currently, there are few DIC $\Delta^{14}C$ measurements for the Arctic Ocean and, to the best of our knowledge, no $\Delta^{14}C$ measurements reported for Baffin Bay. The first seawater $\Delta^{14}C$ profiles measured by Accelerator Mass Spectrometer (AMS), sampling from the Canadian Basin and Eurasian Basin of the Arctic Ocean were taken between 1977 and 1985 (Östlund et al., 1987). DIC $\Delta^{14}C$ values in deep Eurasian Basin are around -60‰ (Östlund et al., 1987), while DIC $\Delta^{14}C$ in the deep Canada Basin are as low as -105‰ (Östlund et al., 1987). The ventilation age of the Eurasian Basin is estimated to be between 10-100 years, and the exchange of water from the Eurasian Basin and Canada Basin is estimated to take between 500 to 800 years (Östlund et al., 1987). $\Delta^{14}C_{bomb}$ was identified in the deep waters of the Eurasian Basin, with $DI^{14}C$ values ranging from -35‰ to +19‰ in the Beaufort Sea, and 52‰ in the Amundsen Basin (Druffel et al., 2017).

DIC $\delta^{13}C$ measurements can be used as water source indicators in the ocean. Isotope fractionation of CO_2 across the air-sea boundary plays a key role in determining DIC $\delta^{13}C$ values. (Sharp, 2007). For examples atmospheric CO_2 contain depleted $\delta^{13}C$ values near -7‰ while marine DIC contain heavier $\delta^{13}C$ values between +1.0 to +1.5‰ due to the preferential uptake of ^{13}C during the exchange of atmosphere-ocean carbon. Photosynthesis produces isotopic fractionation towards more negative $\delta^{13}C$ values. Terrestrial plants have $\delta^{13}C$ values around -27‰ (C3 plants),

whereas marine phytoplankton have $\delta^{13}C$ between -20 to -27‰ (Newton and Bottrell, 2007). High DIC $\delta^{13}C$ values at the surface are the result of high primary production which preferentially removes ^{12}C over ^{13}C from the DIC pool. Decreasing DIC $\delta^{13}C$ values with depth reflect the heterotrophic respiration of sinking particulate organic carbon (Bauch et al., 2015). Surface DIC $\delta^{13}C$ in the Eurasian Basin (+1 to +1.5‰) is only slightly lower than the Canada Basin (+2‰; Bauch et al., 2015). DIC $\delta^{13}C$ in the Canada and Eurasian basin ranges from -0.6 to +2.2‰, with deep waters ranging from +1 to +1.5‰.

Both DIC $\Delta^{14}C$ and $\delta^{13}C$ provide quantitative estimates of carbon sources, anthropogenic and "bomb" atmospheric CO_2 incorporation into the oceans (Quay et al., 2003). DIC $\Delta^{14}C$ can also be used to quantify ventilation rates, water mass aging, and deep water circulation rates (Dutta, 2008). DIC is the largest marine carbon reservoir. DIC $\delta^{13}C$ and $\Delta^{14}C$ measurements have largely shaped our understanding the biogeochemical cycling of this reservoir. Here, I use DIC $\delta^{13}C$ and $\Delta^{14}C$ measurements from Baffin Bay to estimate carbon source inputs, water mass ages, and a ventilation age for the region in hopes of further understanding the Arctic marine carbon cycle and how the region may respond under future climate change.

Using radiocarbon measurements of dissolved inorganic carbon to determine a revised residence time for deep Baffin Bay

A confidential manuscript for submission to Frontiers in Marine Biogeochemistry

Sara Zeidan[1], Jennifer Walker[1], Brent G. T. Else[2], Lisa Miller[3], Kumiko Azetsu-Scott[4], Brett Walker[1*]

[1]Department of Earth and Environmental Science, University of Ottawa, Ottawa, ON Canada K1N 6N5
[2]Department of Geography, University of Calgary, Calgary, AB Canada T2N 1N4
[3]Institute of Ocean Sciences, Fisheries and Oceans Canada, Sydney, BC Canada V8L 4B2
[4]KumikoBedford Institute of Oceanography, Department of Fisheries and Oceans Canada, Dartmouth, NS B2Y 4A2 Canada

**to whom correspondence should be addressed: brett.walker@uottawa.ca*

Abstract

The Arctic Ocean is warming at three times the rate of the rest of the planet and the effect of climate change on the Arctic marine carbon cycle processes remain unconstrained. Baffin Bay is a semi-enclosed, Arctic basin connecting to the Labrador Sea to the south. While the physical oceanography of surface Baffin Bay is well characterized, less is known about deep water formation mechanisms within the Basin. Only a few residence-time estimates for Baffin Bay Deep Water (BBDW) exist and range from 20 to 1450 years. Better residence time estimates are needed to understand how Baffin Bay will respond to climate change. Here we report stable carbon ($\delta^{13}C$) and radiocarbon ($\Delta^{14}C$) values of DIC collected aboard the CCGS *Amundsen* in 2019. We observed DIC $\delta^{13}C$ and $\Delta^{14}C$ values between 0.7‰ to +1.9‰ and -90.0‰ to +29.8‰, respectively. Surface DIC $\delta^{13}C$ values were between +0.7‰ to +1.9‰, while deep (>100m) values were 0.0 to -0.7‰. Surface DIC $\Delta^{14}C$ values ranged between -5.4‰ to +22.9‰, while deep DIC (>1400m) DIC $\Delta^{14}C$ averaged -82.2±8.5‰ (n = 9). In order to constrain natural DIC $\Delta^{14}C$ values, we quantified the amount of atmospheric "bomb" ^{14}C in DIC ($\Delta^{14}C_{bomb}$; using the potential alkalinity method; P_{alk}) and anthropogenic DIC (DIC_{anth}; using the ΔC^* method). Both proxies indicated an absence of $\Delta^{14}C_{bomb}$ and DIC_{anth} below 1000m. Using two previously proposed deep water formation mechanisms and our corrected DIC $\Delta^{14}C_{natural}$ values, we estimated a ^{14}C-based residence time of 360-690 years for BBDW. Based on these residence times, we infer carbon is likely stored for centuries in deep Baffin Bay.

Keywords: **Dissolved inorganic carbon, $\delta^{13}C$, $\Delta^{14}C$, anthropogenic, fossil, bomb, residence time, Baffin Bay**

2. Introduction

Approximately half of the carbon dioxide (CO_2) emitted into the atmosphere from fossil fuels has been absorbed by the oceans. It has been suggested the oceans comprise the only true sink of atmospheric CO_2 over the past 200 years, storing carbon in the deep ocean on timescales of ~1000 years (Sabine et al., 2004). Most of this oceanic carbon is stored as dissolved inorganic carbon (DIC; ~38,000 GtC), the largest marine carbon reservoir (Heinze, 2014). The Arctic Ocean is an important region for the marine carbon cycle (Hamilton and Wu, 2013) and is warming at three times the rate of the rest of the planet (Arctic Monitoring & Assessment Programme Arctic Climate Change Update, 2021). The effect of climate change on the marine carbon cycle in the Arctic and on atmospheric CO_2 remain largely unconstrained.

Previous studies have used available DIC concentration measurements along Arctic gateways coupled with mass transport models to parameterize an Arctic Ocean DIC budget (e.g. MacGilchrist et al., 2014, Olsen et al., 2015), with the Arctic Ocean absorbing roughly 225 ± 49 Tg C yr^{-1} via air-sea gas exchange during the summer months (MacGilchrist et al., 2014). These studies suggest the Arctic Ocean is a carbon sink for most of the year, with open water biological activity accounting for a large portion of CO_2 uptake, while assuming that the sink is limited during the winter by sea ice cover (Shadwick et al., 2011). Many Arctic regions can act as sinks of anthropogenic carbon below the mixed layer, through the export of particulate organic carbon (POC) and downwelling of carbon rich surface waters. While DIC concentration and total alkalinity measurements have played a critical role in our understanding of Arctic carbon cycling and ocean acidification, these studies require significant multiple sampling campaigns and high spatial and temporal measurements to constrain carbon fluxes. Furthermore, most sampling campaigns have been limited to the summer season, limiting air-sea CO_2 exchange estimates to only ice-free seasons (Bates and Mathis, 2009).

A wide range in marine DIC radiocarbon ($\Delta^{14}C$) and stable carbon ($\delta^{13}C$) values can be used as powerful oceanographic tracers of water mass sources, ages, and deep water formation rates. Additionally, the decrease in atmospheric $\delta^{13}CO_2$ (e.g., the Suess effect) has been used as

key evidence for anthropogenic carbon sequestration in the form of marine DIC (Körtzinger et al., 2003). For example, DIC $\delta^{13}C$ values in the Arctic Ocean range between -0.6 and +2.2‰, with deep DIC $\delta^{13}C$ ranging from -1.0 to +2.0‰, in both the Canadian and Eurasian Basins, respectively (Griffith et al., 2012; Bauch et al., 2015). DIC $\delta^{13}C$ values in the Beaufort Sea, which feeds Pacific water to the Canadian Arctic Archipelago (CAA), range between -0.5 to +2.2‰ (Mol., 2017). The North Atlantic Ocean, which receives Arctic water through Davis and Fram Strait, consists of DIC $\delta^{13}C$ between -0.1 to +1.9‰ (Humphreys et al., 2016). These DIC $\delta^{13}C$ values serve as valuable endmembers for understanding DIC cycling in dynamic Arctic Ocean environments.

Only a handful of Arctic DIC $\Delta^{14}C$ measurements have been conducted throughout the Arctic Ocean, with $\Delta^{14}C$ values of -60‰ found in the deep water of the Eurasian Basin, and values as low as -105‰ to -112‰ in the Canadian Deep Basin (Östlund et al., 1987). Surface DIC $\Delta^{14}C$ values range between -35‰ to +19‰ in the Beaufort Sea, and +52‰ was measured at a single station in the Amundsen Basin (Druffel et al., 2017), while deep DIC $\Delta^{14}C$ values in the Beaufort Sea were found as low as -111‰ (Griffith et al., 2012) Aside from these few studies, virtually no other DIC $\Delta^{14}C$ values have been published for the Arctic.

^{14}C is a naturally produced in the stratosphere through the capture of slow cosmic ray neutrons by the atmospheric ^{14}N nuclei (Trumbore et al., 2016). In addition, the infiltration of atmospheric "bomb" CO_2 into the global oceans since the 1960s has made bomb ^{14}C a useful physical oceanographic tracer. Atmospheric $\Delta^{14}C$ values reached +1000‰ after peak nuclear weapons testing. Surface marine DIC $\Delta^{14}C$ peaking at roughly +200‰ a decade later. Atmospheric CO_2 and surface marine DIC $\Delta^{14}C$ values have declined to 0‰ today, due to dilution of this signal via increased fossil fuel output and the incorporation of atmospheric CO_2 into the oceans and terrestrial biosphere (Guilderson et al., 2000; Brown and Reimer, 2004). Similarly, the influx of fossil ($\Delta^{14}C$= -1000‰) CO_2 into the marine DIC reservoir (i.e., the Suess Effect) has proven a useful tool for quantifying anthropogenic impacts on the ocean (Chen and Millero, 1979). However, to the best of our knowledge these $\Delta^{14}C$ estimates have not been made in the Arctic.

In this study, we present the first DIC $\Delta^{14}C$ and new $\delta^{13}C$ data from Baffin Bay. Here we use the dual $\Delta^{14}C$ and $\delta^{13}C$ isotopic value of DIC to trace water mass characteristics, DIC sources, the penetration of bomb vs. anthropogenic (fossil) $\Delta^{14}C$ and to estimate the first ^{14}C-based residence age of Baffin Bay deep water.

3. Methods

3.1 Sample collection

DIC samples for $\delta^{13}C$ and $\Delta^{14}C$ analyses were collected from 11 stations throughout Baffin Bay in July 2019 aboard the icebreaker CCGS *Amundsen* (Figure 1**)**. Water samples were collected throughout the water column for each station using a rosette equipped with the SBE 911plus conductivity, temperature, depth probe (CTD) and 24 × 12L Niskin bottles. Prior to DIC $\Delta^{14}C$ and $\delta^{13}C$ sample collection, 250 mL Pyrex bottles (Corning #1395-250), caps and 45 mm clear pouring rings were cleaned by soaking in 10% HCl for 1 hour, rinsed with copious 18.2 MΩ Milli-Q water (TOC <4ppb) and dried overnight. The bottles were then baked at 540°C for 2 hours. Samples for DIC and Total Alkalinity (A_T) concentrations were collected into 250 mL glass biological oxygen demand (BOD) bottles, overflowed three times, and sealed with Apezion M grease on stone-ground glass stoppers and secured with electrician's tape. Samples were then poisoned with 100µL of saturated $HgCl_2$ and stored in a dark area at room temperature. Samples were analysed following methods set forth by Dickson et al. (2007). Nutrients samples were collected in 20 mL polyethylene flasks and measured immediately at sea.

3.2 DIC, Total Alkalinity, salinity, and nutrient analysis

DIC concentrations were analyzed by coulometry (Johnson et al., 1993) and A_T by open cell potentiometric titration after (Dickson et al., 2007). DIC and A_T samples were analyzed within 15 months of collection at both the Bedford Institute of Oceanography (BIO; stations 193, 196, and 224) and the Institute of Ocean Sciences (IOS; stations BB15, BB18, 227, 224, BB2, 204, 210 108, and 323). Analytical precision was determined by repeated analysis of a bulk seawater; samples analyzed at Bedford Institute of Oceanography, for DIC and A_T was ±0.03%. ±0.05%, respectively. Results for DIC and A_T at IOS were calibrated against certified reference material (CRM) supplied provided by Dr. Andrew Dickson (Scripps Oceanographic Institution, San Diego, USA), and the analytical precision was 1.1 µmol kg^{-1} for DIC and 2.0 µmol kg^{-1} for A_T. An inter-lab comparison of DIC and A_T concentrations yielded errors of ±7.76 µmol kg^{-1} and ±14.27 µmol kg^{-1} (n = 24), respectively. Bottle salinity data was collected from the rosette system and analyzed onboard using an AUTOSAL 8400B salinometer and reported in the Practical Salinity Scale units (PSU). Nutrient concentrations were measured by colorimetry following Aminot & Kérouel, (2007) at Université Laval with an analytical precision of ±1 µmol kg^{-1}.

3.3 Stable isotope ($\delta^{13}C$) analysis

For each sample, 1 mL of seawater was transferred into a pre-cleaned 12 mL Exetainer vials, where vials are flushed with UHP He gas within a glove bag to remove of any atmospheric CO_2. 5.3 mL of 85% H_3PO_4 was then added to each sample, which was shaken and left to equilibrate for at least 12 hours at room temperature. This allowed the DIC to equilibrate with CO_2 in the headspace of the vials (Olack et al., 2018). Isotopic standards were prepared using external calcite and limestone standards (IAEA NBS-18 $\delta^{13}C$ = -5.01‰ and IAEA NBS-19 $\delta^{13}C$ = +1.95). Internal bicarbonate standards ($\delta^{13}C$ = -3.02‰; VL-1, $\delta^{13}C$ = -7.5‰; OXG, Ján Veizer Stable Isotope Laboratory) were also used. DIC $\delta^{13}C$ values were measured using a Thermo-Finnagan Gas Bench coupled to a Thermo-Finnagan Delta V-Plus Continuous Flow Isotope-Ratio Mass Spectrometer (IRMS) at the University of Ottawa, Ján Veizer Stable Isotope Laboratory. Results are reported in standard per mil (‰) notation and relative to Vienna Pee Dee Belemnite (V-PDB) for $\delta^{13}C$. Average external precision based on sample replicates (n = 100) was ±0.1‰.

3.4 Natural abundance radiocarbon ($\Delta^{14}C$) analysis

DIC in seawater samples was extracted as headspace CO_2 for $\Delta^{14}C$ analysis following Gao and co-workers (Gao et al., 2014). Approximately 40 mL of seawater was transferred to pre-cleaned and pre-weighed 60 mL vials (Fisher Scientific #5719398) by decanting in a glove bag flushed multiple times with ultra-high purity (UHP) N_2 gas. Filled 60 mL vials were then sealed with a Viton and silicone septa, secured with a cap, and weighed to get an accurate seawater volume. Each vial was then injected with 0.5 mL of 85% H_3PO_4 (Fisher Scientific # A260500) using a 5mL glass syringe (brand, part #) and a 23-gauge side-port needle (Fisher Scientific #14815488). Acidified samples were gently shaken and heated in a block at 75°C for 2 hours.

Isotopic standards were prepared using in-house carbonate standards (Fm = 0.9444 ±0.0018; Coral STD, UC Irvine), IAEA-C2 travertine (Fm = 0.4114±0.0003), and $NaHCO_3$ (Fm = 0; AEL-AMS lab, uOttawa). Standards were weighed and transferred in a glove bag into pre-cleaned 60 mL I-Chem vials, along with 40 mL of stripped standard water (100 mL of Milli-Q water stripped with UHP N_2 gas for 15 minutes) and sealed. Standards were then acidified with 0.5 mL of 85% H_3PO_4 and heated at 75°C for 2 hours.

Combusted OX-1 (Fm = 1.0398), OX-2 (Fm = 1.3407) standards and in-house Glycine (Fm = 0) were used as modern normalization standards and dead process blank standards during AMS sample analysis. Standards were measured in sealed, pre-baked (baked at 540°C for 2 hrs) 6 mm quartz tubes with ~150 mg of CuO. Quartz tubes containing standards were then combusted at 850°C/3h and expanded into a vacuum line to purify the resultant CO_2. Samples and standards were cryogenically purified, followed by conversion to pure graphite using the sealed-tube Zn method (Xu et al., 2007).

For DIC samples and standards extracted based on the (Gao et al., 2014) method, a pre-flushed 60 mL BD Luer-Lock syringe equipped with a BD 2.5 cm needle was used to extract CO_2 collected in the headspace of each sample and inserted to the beginning of the vacuum line system through a septum. The CO_2 was then cryogenically purified in a -80°C liquid nitrogen and ethanol trap to freeze out any water, followed by a pure liquid nitrogen trap to clear non-condensable gases. The purified CO_2 gas was quantified manometrically and transferred to a Zn reaction tube and flame sealed. Samples were graphitized at 550°C in an oven following Xu and co-workers (2007) and analyzed for $\Delta^{14}C$ at the Keck Carbon Cycle AMS facility at the University of California Irvine. DIC radiocarbon data is reported as Fraction Modern (Fm), $\Delta^{14}C$ and apparent ^{14}C age following the conventions set forth by (Stuiver and Polach, 1977) and corrected for year of sample collection and for modern vs. dead C blanks associated with sample preparation and extraction.

3.5 Estimation of anthropogenic (DIC_{anth}) and "bomb" DIC ^{14}C

It is important to note that our measured DIC $\Delta^{14}C$ values include contributions of both atmospheric "bomb" ^{14}C (from 1950s above-ground thermonuclear weapons testing) and also fossil (anthropogenic) CO_2 that are incorporated into the DIC reservoir through air-sea gas exchange. This multiple source DIC mixture can be expressed in the following simple equation.

(1) $$DIC_{measured}\Delta^{14}C_{measured} = DIC_{natural}\Delta^{14}C_{natural} + DIC_{bomb}\Delta^{14}C_{bomb} + DIC_{anth}\Delta^{14}C_{anth}$$

We use two methods to correct DIC $\Delta^{14}C_{measured}$ values to $\Delta^{14}C_{natural}$ values which can then be used to estimate a ^{14}C-residence time for BBDW.

First, we use the potential alkalinity method (P_{alk}) proposed by (Rubin and Key, 2002). This method separates the amount of $\Delta^{14}C_{bomb}$ from $\Delta^{14}C_{natural}$. P_{alk} is first calculated using measured total alkalinity (A_T), then correcting for biological activity using nitrate concentrations

and normalized to salinity (Equation 2). $\Delta^{14}C_{bomb\ corr}$ was then calculated based on the regression statistics between global $\Delta^{14}C$ versus potential alkalinity measurements (Equation 3) corrected for a global surface potential alkalinity value of 2320, known as P_{alk0}. $\Delta^{14}C_{bomb}$ was determined by calculating the difference between $\Delta^{14}C_{measured}$ and $\Delta^{14}C_{bomb\ corr}$ for each sample.

(2) $$P_{alk} = (A_T + \text{Nitrate}) \times 35/\text{Salinity}$$

(3) $$\Delta^{14}C_{bomb\ corr} = -59.0 - 0.962(P_{alk} - 2320)$$

Second, the amount of anthropogenic carbon present in DIC (DIC_{anth}) was calculated by using the quasi-conservative tracer (ΔC^*) method following methods set forth by (Lee et al., 2003). ΔC^* is calculated as shown in Equation 4 and presented in μmol kg^{-1}. $O_{2\ measured}$ and $O_{2\ eq}$ represent measured oxygen concentrations and oxygen saturation levels at a given temperature and salinity, respectively. A_T is measured alkalinity concentrations, and A_T^0 represents performed alkalinity concentrations as defined by Equation 5. NO represents the relationship between oxygen and nitrate concentrations, as shown in Equation 6. $R_{C:O}$ and $R_{N:O}$ represent the stoichiometric ratios which relate inorganic carbon (C), nitrate (N), and dissolved oxygen (O), and are based on the Redfield Ratio proposed by (Anderson et al., 1994). $DIC_{measured}$ represents total inorganic carbon concentrations, and DIC_{eq} is the DIC in equilibrium with pre-industrial atmospheric CO_2 levels with a fugacity of 280 μatm (Equation 7).

(4) $$\Delta C^* = DIC_{measured} + R_{C:O}(O_{2\,eq} - O_{2\,measured}) - 0.5\left[(A_{T\,measured} - A_T^0) - R_{N:O}(O_{2\,eq} - O_{2\,measured})\right] - DIC_{eq}(fCO_2 = 280\mu atm, A_T^0, \theta, S)$$

(5) $$A_T^0(\mu\text{mol kg}^{-1}) = 335.7 + 55.80 \times S + 0.08924 \times NO$$

(6) $$NO = O_2 - R_{O:N} \times N$$

(7) $$DIC_{eq} = 2077 - 8.517(\theta - 9) + 3.523(S - 35) + 0.6399(A_T^0 - 2320)$$

Final anthropogenic carbon concentrations are calculated from Equation 8, using ΔDIC_{diseq} values from (Lee et al., 2003) based on seawater potential density. DIC_{anth} values <5 μmol kg^{-1} were assumed to contain zero DIC_{anth} (See *Appendix A and B*).

(8) $$DIC_{anth} = \Delta C^* - \Delta DIC_{diseq}$$

Through a comparison of N. Atlantic vs. Baffin Bay DIC_{anth} and $\Delta^{14}C_{bomb}$ depth profiles, we find that the P_{alk} proxy grossly overestimated $\Delta^{14}C_{bomb}$ values for depths shallower than 400m. In general, we found estimated DIC_{anth} values via the ΔC^* proxy gave more realistic values, albeit lower than in the North Atlantic, and sometimes negative. Both proxies were parameterized for

the subtropical N. Atlantic and have recognized limitations for surface high latitude waters (Rubin and Key, 2002; Lee et al., 2003).

To remove DIC_{anth} and DIC_{bomb} $\Delta^{14}C$ contributions from $\Delta^{14}C_{measured}$, a two-endmember mixing model was used to determine the $\Delta^{14}C$ per mil equivalence of DIC_{anth}, which accounted for DIC_{anth}, $DIC_{measured}$, and a $\Delta^{14}C_{anth}$ value of -1000‰ (*see Appendix A and B*). For stations above 500m, only the per mil equivalence DIC_{anth} was subtracted from $\Delta^{14}C_{measured}$. For stations below 500m, both $\Delta^{14}C_{bomb}$ and the per mil equivalence of DIC_{anth} were subtracted from $\Delta^{14}C_{measured}$, to determine $\Delta^{14}C_{natural}$. DIC $\Delta^{14}C_{natural}$ values were converted to a fraction modern (Fm) value and then to an apparent ^{14}C-age based on a half-life of 5730 years. To calculate a residence time of the region, we used DIC $\Delta^{14}C$ and other relevant measurements from the A16N line in the North Atlantic Ocean in 2013 (https://cchdo.ucsd.edu/cruise/33RO20130803). DIC_{anth} and $\Delta^{14}C_{bomb}$ corrections made to $\Delta^{14}C_{natural}$ values and a corrected apparent ^{14}C-age.

4. Results

4.1 DIC $\delta^{13}C$ values

DIC $\delta^{13}C$ values ranged from -0.7‰ to +1.9‰ across Baffin Bay (Figure 2a**)**. Positive DIC $\delta^{13}C$ values were observed at surface depths (+0.7‰ to +1.9‰) and negative DIC $\delta^{13}C$ were observed at depths greater than 100m (-0.0‰ to -0.7‰). Surface DIC $\delta^{13}C$ values (less than 20m) were highest along the coast of Greenland and in the Northern gateways (stations BB18, 227, 210, 108 and 323; $\delta^{13}C$ = +1.3±0.4‰, *n* = 12), while lower values were found along Davis Strait and central Baffin Bay (stations 193, 196, BB2, and 224; $\delta^{13}C$ = +0.9±0.3‰, *n* = 8). Mid-depth (200 – 700m) DIC $\delta^{13}C$ ranged from -0.4‰ to +0.2‰, with slightly more negative values found at stations BB18 and 227 ($\delta^{13}C$ = -0.30±0.07‰; *n* = 4). Below 750m in Baffin Bay, DIC $\delta^{13}C$ values had a narrow range (-0.28±0.16‰; *n* = 19). Deep water (>1200m) at Station 224 was more negative (-0.51±0.11‰; *n* = 4) than DIC $\delta^{13}C$ values at station BB2 (-0.27±0.07‰; *n* = 4).

4.2 DIC $\Delta^{14}C$ values

Our measured Baffin Bay DIC $\Delta^{14}C$ values had a ~120‰ range (from –90.0‰ to +29.8‰; Figure 2b). Surface (less than 20m) DIC $\Delta^{14}C$ values ranged between -5.4‰ to +22.9‰. Positive surface DIC $\Delta^{14}C$ were found along coastal Greenland (stations 196, BB15, BB18, 227 204, and

210; $\Delta^{14}C$ = +17.6±2.5‰, *n* = 12). In contrast, more negative DIC $\Delta^{14}C$ surface values were found in the Northern gateways (stations 108 and 323; $\Delta^{14}C$ = -1.7±3.3‰, *n* = 3). Surface DIC $\Delta^{14}C$ values at central stations (193, BB2, 224) fell between these two end members ($\Delta^{14}C$ = +8.5±3.7‰; *n* = 6). Mid-depth waters (200 – 700m) had DIC $\Delta^{14}C$ between -1.11‰ and +29.8‰, with more positive $\Delta^{14}C$ values found in Northern Baffin Bay (stations BB2, 108, and 323; $\Delta^{14}C$ = +23.8±3.9‰, *n* = 7). Below 750m, DIC $\Delta^{14}C$ values gradually decreased from +7.7‰ to –90.0‰, with the deepest water (1400 – 2400m) having the most negative $\Delta^{14}C$ values (-82.2±8.5‰; *n* = 9).

5. Discussion

5.1 Baffin Bay – hydrographic setting

At the time of sampling, wide ranges in Baffin Bay surface water salinity and temperature were observed (Figure 3a). Surface water (above 50m) on the western side of Baffin Bay was cooler and fresher, while surface water on the eastern side was warmer and more saline (Fox and Walker, submitted). These surface water summer conditions are influenced by surface processes such as solar insulation, wind-driven mixing, and ice melt (Fissel et al., 1982). Surface water variance is also influenced by the current systems within Baffin Bay.

Two main currents are dominant in Baffin Bay: the Baffin Island Current (BIC) and the West Greenland Current (WGC). The BIC is a southerly flowing current containing Arctic Water (AW) to depths of 300m and has water temperatures <-1.6°C and salinities <33.8 (Münchow et al., 2015). AW enters Baffin Bay via the Northern Gateways (Nares Strait and Lancaster Sound) and is modified through glacial and sea ice discharge (Curry et al., 2011). In this study, AW was observed at both central stations (BB2, 224) between 100-300m. Western Greenland Shelf Water (WGSW) was evident along the coast of Greenland and was both warm (7°C) and saline (34.1), with a density anomaly ($\sigma_\theta = \rho_\theta - 1000$, where ρ is density and θ indicates potential temperature) ranging between 25.5 and 27.3 kg m^{-3}. WGSW is composed of waters from the East Greenland Current (EGC), which originate from Arctic water exiting through Fram Strait and later enter Baffin Bay via the WGC (Cuny et al., 2002). As the WGSW progresses northward along the WGC extension, it becomes fresher and cooler, due to mixing with glacial meltwater (Münchow et al., 2015).

At depth, several water masses are present in Baffin Bay. West Greenland Irminger Water (WGIW) is defined by salinities >34.1, potential temperatures >2°C, and a density range of 27.3 to 28 kg m^{-3} (Curry et al., 2011). WGIW originates from warm, saline water found in the Irminger Sea. Transitional Water (TrW) found below 250m, is modified Arctic water that has mixed with WGIW (Curry et al., 2011). The TrW typically has temperatures >2°C, salinities <33.7, and σ_θ of 25.5 – 27.3kg m^{-3} (Curry et al., 2011). Baffin Bay Deep Water (BBDW) has a temperature and salinity of 0°C and ~34.5, respectively, and is found between 1200 and 1800m (Curry et al., 2011). Baffin Bay Bottom Water (BBBW) has a temperature and salinity of -0.4°C and ~34.5, respectively. These deep water masses are more difficult to distinguish using temperature, salinity, and water mass density alone (Lehmann et al., 2019).

5.2 DIC $\delta^{13}C$ as a water mass tracer

DIC $\delta^{13}C$ values in Baffin Bay generally follow depth trends consistent with those observed in the open ocean. Surface DIC $\delta^{13}C$ values are positive, whereas deep DIC $\delta^{13}C$ values are negative (Figures 2a and 3b). These trends in DIC $\delta^{13}C$ are attributed to air-sea gas exchange with some isotopic fractionation of CO_2 across the air-liquid boundary and to a much lesser extent the fractionation of organic carbon through photosynthesis (Zhang et al., 1995). Negative DIC $\delta^{13}C$ values at depth can be attributed to fractionation during the slow remineralization of sinking particulate and dissolved organic matter (POM; DOM) via heterotrophic respiration. Older aged water masses typically contain more negative DIC $\delta^{13}C$ values, since there is more time for remineralization (Kroopnick, 1985; Emerson and Hedges, 2008). The spatial distribution of DIC $\delta^{13}C$ values also provide useful constraints on possible DIC sources. For example, in Baffin Bay there are several possible DIC sources present in both the BIC and WGC, including: Pacific, North Atlantic, Arctic water, regional sea ice melt and glacial melt water. Since deep water DIC $\delta^{13}C$ values were largely invariant, here we focus our discussion on surface and intermediate water DIC $\delta^{13}C$ values.

Surface (above 20m) DIC $\delta^{13}C$ is highly variable in Baffin Bay. The warm surface WGSW along the coast of Greenland contains higher DIC $\delta^{13}C$ values (>+1.03‰). These values are consistent with previously reported DIC $\delta^{13}C$ from the North Atlantic along the southern tip of Greenland (+1.09 to +1.90‰; (Humphreys et al., 2016)). Within WGSW, we observe an increase in surface DIC $\delta^{13}C$ values from station 196 to 210 (+1.03 to +1.90‰, respectively). One possible

explanation for this trend is high nutrient loading from significant glacial melt along the coast of Western Greenland, leading to enhanced primary production and positive DIC $\delta^{13}C$ fractionation as the water flows north. For example, station BB18, located in the Viagat Fjord behind Disko Island, had the highest surface DIC $\delta^{13}C$ (+1.90‰). This station also had high POM and chlorophyll-*a* concentrations due to an abundance of diatoms (*Walker unpublished data, Lovejoy pers. comm.*). This marginal sea ice region and the inflow of saline Atlantic water have been previously shown to promote primary production (Krawczyk et al., 2021).

Northern Gateway stations (108 and 323) had high surface DIC $\delta^{13}C$ values (+0.71 to +1.42‰). Surface water in Smith Sound (Station 108) is a mixture of both the inflow of Arctic water from Nares Strait and WGSW (Hamilton and Wu, 2013). Therefore this station does not represent a pure Arctic water endmember. Surface water in Lancaster Sound (Station 323) contains Pacific Water entering Baffin Bay via the Canadian Arctic Archipelago. High surface DIC $\delta^{13}C$ values in Lancaster Sound may be indicative of this Pacific influence, which has been observed to have DIC $\delta^{13}C$ values up to +2.20% in the Amundsen Gulf (Mol., 2017). Lancaster Sound is also a region of seasonal sea ice cover, which contribute to high primary production and diatom species richness from nutrient input (Krawczyk et al., 2021). Together, these factors likely contribute to the high surface DIC $\delta^{13}C$ values we observed at Station 323. High variability in surface DIC $\delta^{13}C$ in Baffin Bay can be attributed to varying sea ice and glacial melt contributions, as evident in large ranges in observed surface salinity as shown in Figure 3a. These contributions and upwelling may also promote primary production and indirectly result in high DIC $\delta^{13}C$ values.

Central Baffin Bay stations BB2 and 224 had lower surface DIC $\delta^{13}C$ values (+1.06 to +1.50‰) than Eastern Baffin Bay stations along coastal Greenland (Figure 3). These lower DIC $\delta^{13}C$ values appear to coincide with the presence of Arctic water within the BIC. The Arctic Ocean is covered in sea ice for most of the year, inhibiting air-sea gas exchange and increasing the time in which heterotrophic respiration can act to lower DIC $\delta^{13}C$ values (Morée et al., 2018). DIC $\delta^{13}C$ values within the BIC (20 – 200m; 0.07 – 0.37‰) are significantly higher than that of WGIW (-0.39 to +0.07‰), reflecting more recent air-sea gas exchange in the BIC vs. older, intermediate water (Münchow et al., 2015).

Overall, the trends we observe in DIC $\delta^{13}C$ values in temperature-salinity space (Figure 3b) suggest that DIC $\delta^{13}C$ can be used as an effective tool for distinguishing carbon sources within water masses. A simple least squares regression of DIC $\delta^{13}C$ (y) and potential density (x) resulted

in statistically significant correlations at all stations in Baffin Bay; in particular for coastal Greenland (R^2=0.78-0.98) and Northern Gateways stations (R^2=0.85-0.96; see Table B1 and Figure B1 and Figure B3). Surface DIC $\delta^{13}C$ variability is strongly affected by sea ice melt (more positive DIC $\delta^{13}C$) and the inflow of saline Atlantic water (more negative $\delta^{13}C$). This is especially true for several coastal Greenland stations adjacent to large Fjord regions (Stations BB18, 227, 210; Figure B4 and Table B3). In contrast, deep DIC $\delta^{13}C$ variability is driven by slow heterotrophic respiration at depth. This is indicated by lighter DIC $\delta^{13}C$ values with depth (>1000m, σ_θ = ~27.7 kg/m^3) at the deeper stations 224 and BB2 (-0.27 to -0.68‰ at 1000 to 2000m and -0.16 to -0.36‰ at 1200 to 2300m, respectively).

5.3 DIC $\Delta^{14}C$ distributions in Baffin Bay

We observe a wide range in DIC $\Delta^{14}C$ values within Baffin Bay (-90.0‰ to +29.8‰; Figure 2B). DIC $\Delta^{14}C$ values can reflect water mass aging via radioactive decay, varying degrees of recent air-sea gas exchange. Allochthonous $\Delta^{14}C$ sources can also influence on DIC $\Delta^{14}C$ values. For example, the advection of waters with different ^{14}C reservoir ages and/or surface vs. atmospheric $\Delta^{14}C$ offsets. With deep-water formation, modern surface DIC $\Delta^{14}C$ can also contribute to observed deep ocean DIC $\Delta^{14}C$ values (e.g., the North Atlantic Ocean; Broecker et al., 1960).

Surface (above 20m) DIC $\Delta^{14}C$ ranged between -5.4‰ to +22.9‰. Surface DIC $\Delta^{14}C$ values at Greenland stations (196, BB15, 227, 204, 210) had the most positive DIC $\Delta^{14}C$ values (+14.3‰ to +22.9‰). These values represent positive DIC $\Delta^{14}C$ endmembers from the North Atlantic Ocean at depths <150m (+30.2‰ to +62.3‰; Bullister and Barigner 2020), indicating the WGSW has a large impact on DIC $\Delta^{14}C$ values in Eastern Baffin Bay. Previous studies have noted summer upwelling of warmer, saline WGSW along Greenland (Melling et al., 2010) which would clearly contribute DIC with positive $\Delta^{14}C$ values.

Surface water (above 20m) at the Northern gateways stations (108, 323) had far lower DIC $\Delta^{14}C$ values (-5.4‰ to +0.9‰). These stations contain Arctic and Canadian Archipelago contributions to the Smith and Lancaster Sounds, respectively. Surface DIC $\Delta^{14}C$ values in the Amundsen Gulf and Beaufort Sea range between -35‰ to +19‰, whereas those from the Eurasian Basin are +52‰ (Druffel et al., 2017). Thus, the lower DIC $\Delta^{14}C$ values we observe at station 323 are consistent with advection of Pacific water with low DIC $\Delta^{14}C$ to Baffin Bay from the Canadian

Archipelago. Pacific water nutrient contributions to Baffin Bay were recently reported (Lehmann et al., 2019), again suggesting this is a plausible explanation for our low Station 323 DIC $\Delta^{14}C$ values.

The low DIC $\Delta^{14}C$ values we observe for the Smith Sound (Station 108) are likely impacted by both Arctic Water entering from the Lincoln Sea and WGC water. While no DIC $\Delta^{14}C$ data exist for the Lincoln Sea endmember, this station experiences extended periods of sea ice cover – inhibiting air-sea gas exchange and likely resulting in lower surface DIC $\Delta^{14}C$ values. For our two deep stations (BB2, 224), large gradients in DIC $\Delta^{14}C$ values (-90.0 to +20.6‰) were present in deep (>500m) water of similar densities (σ_θ = 27.56 to 27.72 kg m^{-3}). The surface DIC $\Delta^{14}C$ values we observe in central Baffin Bay are modern (BB2, 224; +5.8‰ to +15.7‰) and possibly comprise a mixture of low Arctic Ocean DIC $\Delta^{14}C$ with positive DIC $\Delta^{14}C$ from WGSW and the influence of seasonal sea ice cover.

Below 1200m, DIC $\Delta^{14}C$ values in central Baffin Bay gradually decrease to-90.0‰ to -35.4‰ (or 225 to 675 ^{14}C-years) at water mass σ_θ of 27.70±0.02 kg m^{-3} (BBDW). Unlike DIC $\delta^{13}C$, no significant relationships were found between potential density and DIC $\Delta^{14}C$ (Table B2 Figure B2). This is because similar, modern DIC $\Delta^{14}C$ values were measured across large surface salinity (and density) gradients. Conversely, at our two deep stations (BB2, 224), large gradients in DIC $\Delta^{14}C$ values were present in mid-depth (500-1200 m) waters of similar σ_θ (e.g., 27.7 kg m^{-3}; Figures 2B, B2).

While the distributions of DIC $\Delta^{14}C$ appear consistent with the physical oceanography of Baffin Bay, DIC $\Delta^{14}C$ values can also be influenced by two anthropogenic $\Delta^{14}C$ contributions. Atmospheric "bomb" $^{14}CO_2$ has increased oceanic $\Delta^{14}C$ values (Mahadevan, 2001; Sweeney et al., 2007). Additionally, ^{14}C-free ($\Delta^{14}C$ = -1000‰) anthropogenic fossil fuel emissions (C_{anth}) have decreased DIC $\Delta^{14}C$ (Carter et al., 2019). The contribution of DIC_{anth} and $\Delta^{14}C_{bomb}$ are ever present in the modern global surface ocean, but their relative contributions and depth of infiltration in the water column vary widely. Since our ultimate goal is to derive a ^{14}C-based residence age of Baffin Bay, we next quantify these contributions to deep Baffin Bay water in order to determine $\Delta^{14}C_{natural}$ and a ^{14}C-residence time.

5.4 Estimation of DIC $\Delta^{14}C_{bomb}$ contributions

Our estimates of $\Delta^{14}C_{bomb}$ using the P_{alk} method (see *section 2.5*) for Station BB2 are shown in Figure 4. Both DIC $\Delta^{14}C_{bomb}$ and $\Delta^{14}C_{bomb\ corr}$ values derived from the P_{alk} method are highly unconstrained above 400m. That is to say that estimated $\Delta^{14}C_{bomb\ corr}$ values are highly negative and estimated $\Delta^{14}C_{bomb}$ values are highly positive, beyond what is reasonably expected for these DIC $\Delta^{14}C$ depth profiles. This is a known limitation of the P_{alk} proxy which was parameterized for low latitude Atlantic waters (<60°N/S). Subtropical Atlantic surface salinities average 36.31±0.35, and surface alkalinity averages 2377±22 µmol kg^{-1} (Jiang et al., 2014). In comparison, surface Baffin Bay salinity and total alkalinity values average 32.2±1.2 and 2194±59 µmol kg^{-1}, respectively. The lower surface salinity and alkalinity values, combined with seasonal sea ice cover and air-sea gas exchange in Baffin Bay, limit the applicability of the P_{alk} method in Arctic waters. The overestimation of bomb $\Delta^{14}C$ above 400m in Baffin Bay is particularly telling. At their peak, global surface DIC $\Delta^{14}C$ values reached +200‰ in the late 1960s (Rodgers et al., 2000). We note that (Rubin and Key, 2002) recognized the P_{alk} proxy predicts lower than expected $\Delta^{14}C_{bomb\ corr}$ values above 58°N and suggested a more reliable calibration value (P_{alk0}) of 2330 µmol kg^{-1} for high latitudes. However, we find surface $\Delta^{14}C_{bomb\ corr}$ values to remain unconstrained even using this P_{alk0} value and that more work is needed to refine the P_{alk} proxy in Arctic waters.

Despite the unconstrained surface estimates of $\Delta^{14}C_{bomb}$ and $\Delta^{14}C_{bomb\ corr}$, at depth we find our these $\Delta^{14}C$ parameters converge with measured DIC $\Delta^{14}C$ values (Figure 4). The confluence of modeled vs. measured values suggests the P_{alk} proxy can accurately predict $\Delta^{14}C_{bomb\ corr}$ at depth, and that $\Delta^{14}C_{bomb}$ is notably absent in BBDW and BBBW. We believe the reliability of the P_{alk} proxy below 400m can be attributed to the similar salinity and alkalinity values in North Atlantic Deep Water (NADW) and deep Baffin Bay. For example, NADW below 1200m (35°N to Equator) has average salinity and alkalinity values of 35.4±1.1 and 2371±37 µmol kg^{-1}, respectively (Takahashi et al., 1981). Average salinity and total alkalinity values below 1000m in BBDW are very similar – 34.39±0.01 and 2290±13 µmol kg^{-1}, respectively. Ultimately, since we estimate no $\Delta^{14}C_{bomb}$ below 1400m, there is no need to correct our deepest measured DIC $\Delta^{14}C$ values for $\Delta^{14}C_{bomb}$ when determining a ^{14}C-based residence time.

5.5 Estimating anthropogenic DIC contributions

Estimated DIC_{anth} concentrations suggest an input of DIC_{anth} primarily from Davis Sill Strait (Figure 5). We calculated DIC_{anth} = 25 - 40 µmol kg^{-1} above 400m at Station 193 and DIC_{anth} = 20 - 33 µmol kg^{-1} at 0-100m at station 196 in Davis Strait (Figure 5A/B; Appendix Table A2). DIC_{anth} enters Davis Strait via the WGC and advects north within WGSW into central Baffin Bay. Davis Strait DIC_{anth} concentrations are only slightly lower than those previously reported for the North Atlantic (Lee et al., 2003), and the North Atlantic supplies significant DIC_{anth} to Baffin Bay. DIC_{anth} contributions were lower at our Northern Gateway stations 108 and 323 (9.4 to 41.5 µmol kg^{-1}), and no DIC_{anth} was found below 100m at these stations. Between 150-300m the southward BIC also contains little DIC_{anth}.

Although we are the first to apply the ΔC^* proxy to the Arctic Ocean, Earth System models estimate low DIC_{anth} inventories due to seasonal sea ice and limited air-sea gas exchange (Tjiputra et al., 2010). Lee and co-workers (2003) also found low DIC_{anth} inventories in surface waters at higher Atlantic Ocean latitudes (~65°N). Low DIC_{anth} at higher latitudes may be attributed to seasonal sea ice cover and reduced air-sea gas exchange, but also to mixing of intermediate waters with deeper DIC_{anth}-free water. In addition to limited air-sea gas exchanged due to sea ice, short residence times (~2 years) of surface water within Baffin Bay may also limit the region's surface DIC_{anth} inventories (Rudels, 1986; Poisson and Chen, 1987; Hoppema et al., 2001). Large volumes of water are annually exported south through Davis Strait (2.3±0.7 Sv; Curry et al., 2011) perhaps also precluding the BIC from containing significant DIC_{anth} (Figure 5).

Above 50m, $_{DI}C_{anth}$ is variable in Baffin Bay. High DIC_{anth} is found in surface water along the coast of Greenland (29-46 µmol kg^{-1}) while, surface DIC_{anth} was not found near Disko Island (BB18) and on the west side of Davis Strait (193). Such wide-ranging DIC_{anth} demonstrates limitations in the ΔC^* proxy for low temperature and salinity waters. As was the case with the P_{alk} method, the ΔC^* proxy was developed for the mid-latitude open oceans. As a result, many of our surface DIC_{anth} values had high errors and/or negative values. The ΔC^* proxy however appears to provide more dependable estimates of surface Arctic waters than the P_{alk} method for $\Delta^{14}C_{bomb}$. With the limitation of the P_{alk} method throughout Baffin Bay surface water, one can assume the absence of $\Delta^{14}C_{bomb}$ when DIC_{anth} is undetectable. As mentioned in *section 2.5*, DIC_{anth} values <5µmol kg^{-1} (including negative values) were considered free of DIC_{anth} and set equal to 0 µmol kg^{-1}. Despite these surface DIC_{anth} proxy limitations, we do not observe the presences of DIC_{anth}

in Baffin Bay below 800m. We believe this to be reasonable given the absence of $\Delta^{14}C_{bomb}$ in BBDW. Thus, our deep water measured DIC $\Delta^{14}C$ values do not require further correction for the addition of fossil C.

5.6 Estimating a ^{14}C-based residence age estimates for deep Baffin Bay

The formation of BBDW and BBBW is topic of ongoing scientific debate. Two main formation mechanisms have been proposed: mixing of cold, saline, brine-enriched surface shelf water with 1) Arctic Intermediate water in Nares Strait and Smith Sound (Collin, 1965; Bailey, 1956; Bourke et al., 1989; Bourke and Paquette, 1991) or 2) Labrador Sea intermediate water entering via Davis Strait (Tang et al., 2004). Some research has argued that the depth of convective mixing from freezing would be too shallow (<100m) to produce the bottom water in Northern Baffin Bay (Muench, 1970), but others have noted this would not preclude downslope transport of dense water from northern shelves (Tang et al., 2004).

In order to constrain a ^{14}C-residence age for deep Baffin Bay, it is important to consider each of these formation mechanisms carefully. The addition of winter brine to Arctic Water at intermediate depths in Smith Sound has been previously supported by temperature, salinity and $\delta^{18}O$ isotopic data (Bailey, 1956; Tan and Strain, 1980). Nares Strait is a relatively shallow region (~200m in Kane Basin). Bottom potential density anomaly at Station 108 was 27.27 kg m^{-3} (225 m depth), which would not be dense enough to contribute directly to Baffin Bay deep water (σ_θ = 27.72 kg/m^3). However, Bourke and co-workers (1989) suggested that mixing brine-enriched winter waters produced in the North Water Polynya in Smith Sound, with Arctic Intermediate could produce deep water densities. If we use natural DIC $\Delta^{14}C$ values from 200-300 m at Station 108 (where C_{ath} was not detected and presumably little bomb $\Delta^{14}C$ is present; Table A2) as a deep water source endmember ($\Delta^{14}C$ = +26.3‰; n = 2), then the ^{14}C residence time of BBDW (σ_θ > 27.7 kg/m^3, $\Delta^{14}C$ = -90.7‰) would be roughly approximate its apparent ^{14}C age (690 ±35 years).

The second plausible source of BBDW is dense water entering Davis Strait from the Labrador Sea over a 640m depth sill. Sverdrup et al., (1942) suggested the cooling of Labrador Sea deep water with winter surface water brine as a formation mechanism. The WGC is cooler and fresher than the EGC (3.0°C < θ < 5.5°C and 34.4 < S < 35.0) or the Irminger Current (3.5°C < θ < 5.5°C, S ~ 35.0; Lobb, 2004). In the northern Labrador Sea, the Irminger current lies below the WGC (Rykova et al., 2009). As it flows northwardly, the upper portion of the Irminger Current

mixes with the cooler and fresher WGC (Cuny et al., 2002). Inflow of WGIW via Davis Strait is seasonal and extends to depth of up to 1000m during the fall (Curry et al., 2014).

We use North Atlantic DIC $\Delta^{14}C$ values (A16N GO-SHIP, Station 4; Bullister and Barigner 2020) from the Davis Strait sill depth (640m) with a density anomaly (σ_θ = 27.53 to 27.67 kg m^{-3}) similar to that of BBDW as a second source endmember from which to estimate a ^{14}C residence time for Baffin Bay. We applied both the P_{alk} and ΔC^* proxies to correct for $\Delta^{14}C_{bomb}$ and DIC_{anth}, respectively from measured North Atlantic DIC $\Delta^{14}C$ to determine a $\Delta^{14}C_{natural}$ depth profile (GO-Ship A16 cruise, Station 4; Figure 6). We note that both proxies provided robust estimates of $\Delta^{14}C_{bomb}$ and DIC_{anth} for the North Atlantic station, consistent with previously published values (Rubin and Key, 2002; Lee et al., 2003). This North Atlantic BBDW source end-member was calculated to have a ^{14}C age of 330 ±35 years. Subtracting this age from the apparent ^{14}C age of BBDW (690 ±35 years) results in an estimated ^{14}C residence time of estimated at 360 ±35 years. Since both bomb $\Delta^{14}C$ and DIC_{anth} are present in the North Atlantic (Rubin and Key, 2002; Lee et al., 2003), in order to have no bomb $\Delta^{14}C$ or DIC_{anth} in BBDW, this mechanism requires extremely slow rates of deep water formation.

Our two estimated ^{14}C residence times (350-690 years) for deep Baffin Bay provide new constraints on the ventilation age of this ocean basin. Our residence times fall between those previously estimated for BBDW of 20 to 1,450 years (Sadler., 1976; Top et al., 1980; Wallace, 1985). It is important to note that both deep water formation mechanisms require cooling and brine rejection during sea ice formation that would increase the local DIC concentration of underlying waters (Köenig et al., 2018; Rysgaard et al., 2007; Moreau et al., 2016). This increase in DIC would also selectively preconcentrate DIC with modern $\Delta^{14}C$ (atmospheric), $\Delta^{14}C_{bomb}$, and fossil (C_{anth}) $\Delta^{14}C$ values. Since we do not detect these $\Delta^{14}C$ endmembers in BBDW, significant dilution must occur during such a deep water formation mechanism (e.g. “shaving” of the deep water plume; Bourke et al 1989). This would also suggest that our estimated ^{14}C residence times are, in fact, minimum age estimates. Nevertheless, with a minimum residence time of 360 ±35years, Baffin Bay stores carbon on centennial timescales longer than deep water found in the Atlantic and Indian Oceans (residence times of 275 and 250 years, respectively; Stuiver et al., 1983).

6. Summary and Implications

Seawater DIC $\delta^{13}C$ and $\Delta^{14}C$ values reveal sources and cycling of carbon in the Arctic. Baffin Bay is a dynamic region, consisting of carbon sources from the Arctic, Pacific, and Atlantic oceans, as well as glacial and terrestrial inputs along the coast of Greenland. $\Delta^{14}C_{bomb}$ and DIC_{anth} estimates through the ΔC^* and P_{alk} proxies are limited in their scope of application in the Arctic but highlight important DIC source constraints to Baffin Bay water masses. A bimodal distribution of DIC_{anth} was observed; DIC_{anth} replete water entering from the North Atlantic Ocean and DIC_{anth} depleted Arctic water in Northern Baffin Bay, while no DIC_{anth} or bomb $\Delta^{14}C$ was found for BBDW. Using two possible deep water formation mechanisms for Baffin Bay, we determine a BBDW ^{14}C residence time of 360-690 years, suggesting deep Baffin Bay stores carbon for several centuries.

Baffin Bay exports cold, dense water to the Labrador Sea which is critical for North Atlantic Deep Water (NADW) formation (Goosse et al., 1997). Global climate change has resulted in warming and freshening of Arctic surface water exported through Baffin Bay and increased stratification in the North Atlantic Ocean. This stratification is now reducing NADW formation (2021 nature paper). We now observe increased CO_2 uptake throughout the Arctic Ocean from reduced sea ice and warming temperatures (MacGilchrist et al., 2014). With a residence time of 360-690 years, Baffin Bay could partially moderate Arctic climate change through storage of deep carbon on centennial timescales.

7. Acknowledgments

We gratefully acknowledge Chief Scientist Alexandre Forest, Anissa Merzouk and the staff of Amundsen Science and the crew of the CCGS Amundsen for the opportunity to participate in the 2019 research cruise. We also would like to thank Dr. Cara Manning for her help in coordinating the sampling and logistics of the Biogeochemistry groups aboard the CCGS *Amundsen*. We thank Tonya Burgers (University of Manitoba) and Shawn Marriott (University of Calgary) for DIC and A_T sample collection and Danielle Caleb and Marty Davelaar (Institute of Ocean Sciences) for sample analyses. We thank Drs. Xiaomei Xu and John Southon of the UC Irvine Keck Carbon Cycle AMS lab for their expertise and help with ^{14}C analysis of our graphite targets. We thank Paul Middlestead and the staff of the Ján Veizer Stable Isotope Laboratory at

the University of Ottawa for aiding in $\delta^{13}C$ analysis of seawater DIC. We thank Jonathan Gagnon and Jean-Éric Tremblay (Université Laval) for nutrient measurements. This work was supported by NSERC (Natural Sciences and Engineering Research Council of Canada) Discovery Grant (B.D.W, B.G.T.E.), the Canada Research Chairs program (B.D.W.), the NSERC Alexander Graham Bell Canadian Graduate Scholarship (S.Z.), the Ontario Graduate Scholarship (S.Z.), and Fisheries and Oceans Canada. This work is a contribution to ArcticNet, a Network of Centres of Excellence Canada.

8. Data availability

The data that support the findings of this study are available in Appendix A and B files and from the corresponding author upon reasonable request.

9. Figures and Captions

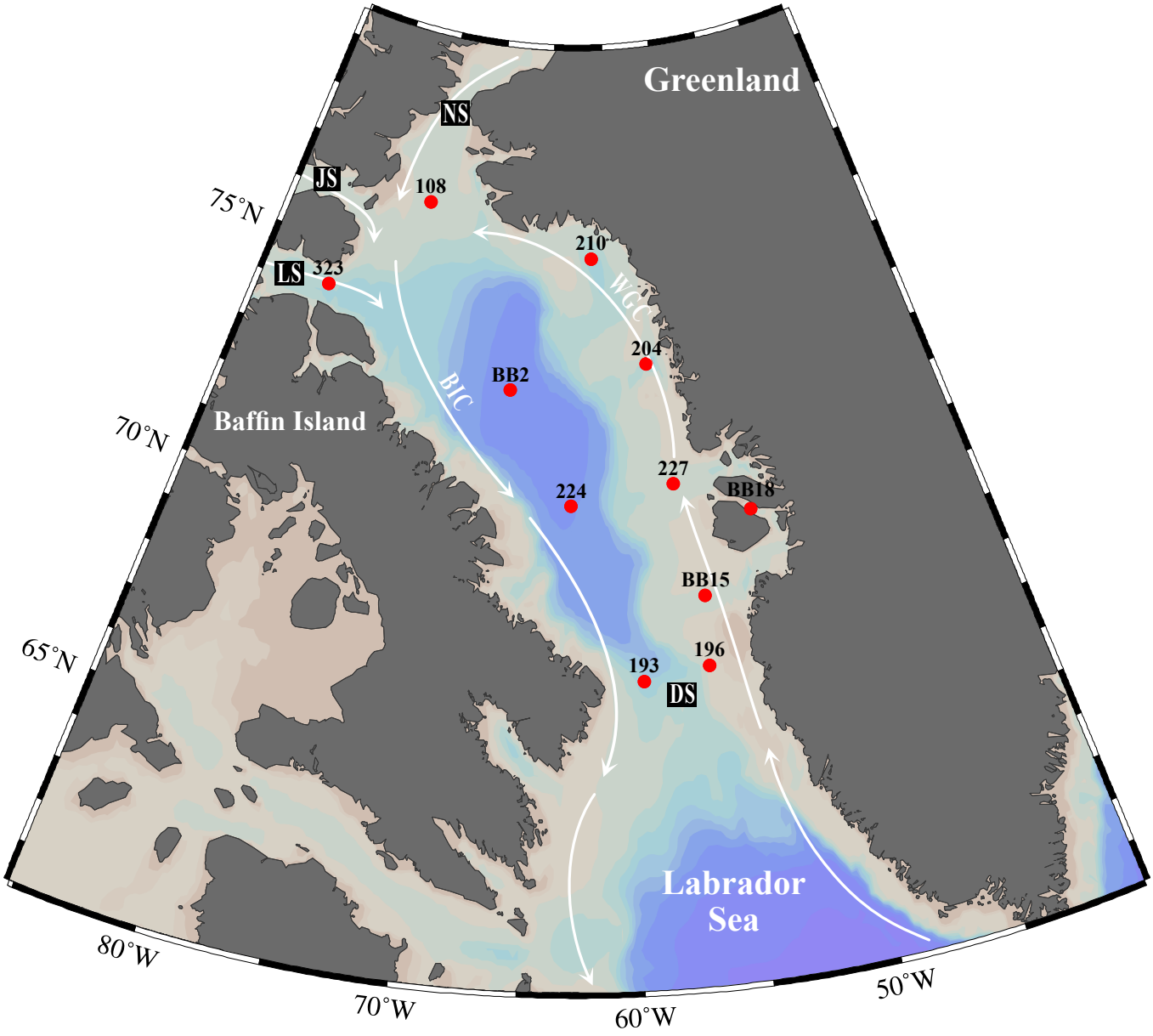

Figure 1. Sample locations, gateways and currents of Baffin Bay. Stations are indicated by red circles, and major currents are indicated by white arrows. Gateways in Baffin Bay are indicated by black boxes and include Davis Strait (DS; 640m deep), Nares Strait (NS; 250m), Jones Sound (JS; 120m), and Lancaster Sound (LS; 125m).

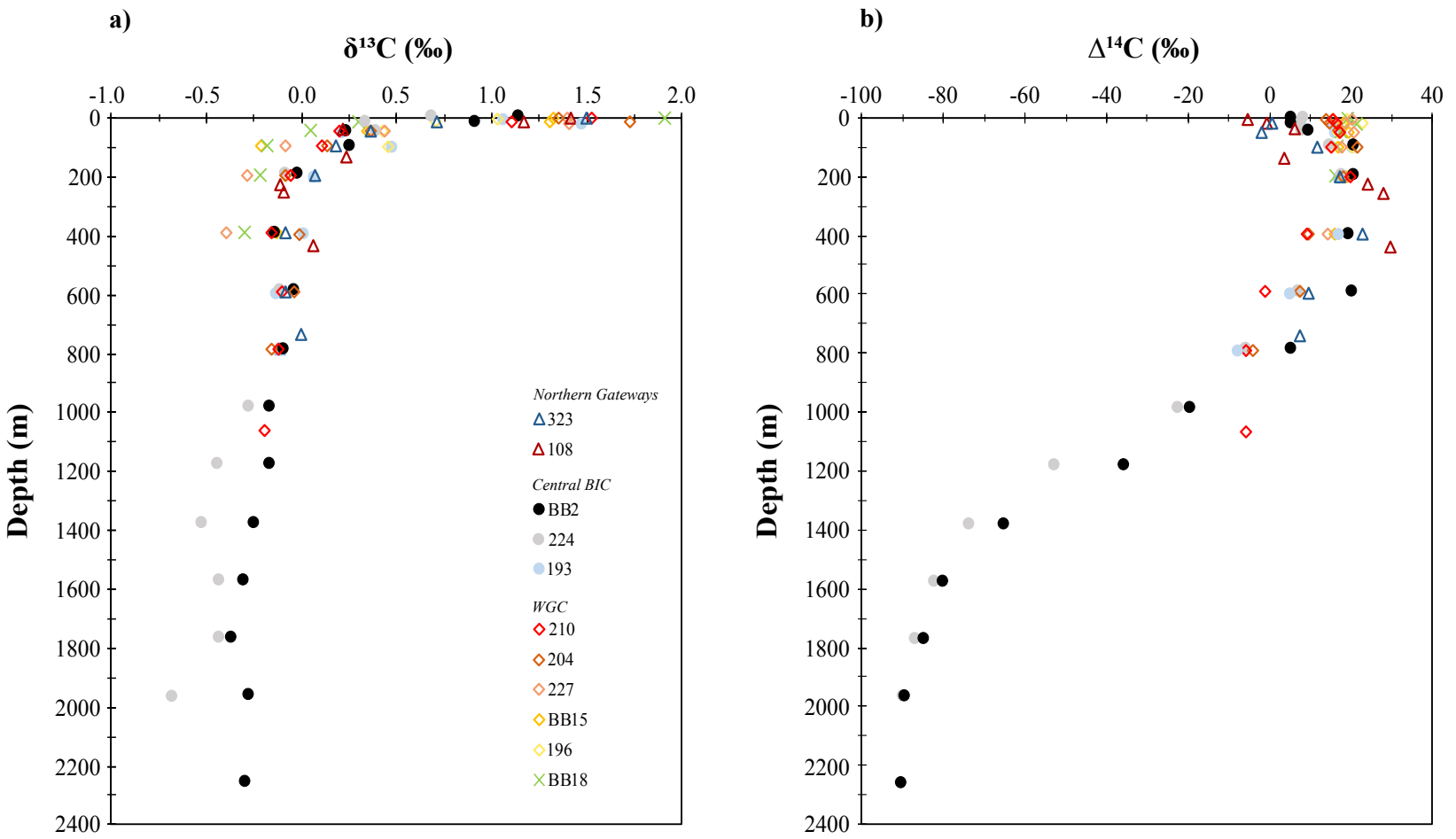

Figure 2. Depth profiles of DIC $\delta^{13}C$ and $\Delta^{14}C$ values in Baffin Bay. a) measured DIC $\delta^{13}C$ values, ± 0.1‰ (See section 2.3). Different sampled stations (Figure 1) indicated by legend, which cover the extent of the Baffin Island Current (BIC) in central Baffin Bay (circles), the Western Greenland Current (WGC) along the coast of Greenland, (diamonds). and the Northern gateways of Nares Strait and Lancaster Sound (triangles). **b)** DIC $\Delta^{14}C$ signatures, with errors ranging between 1.2 to 2.0‰ (See sections 2.4-2.5).

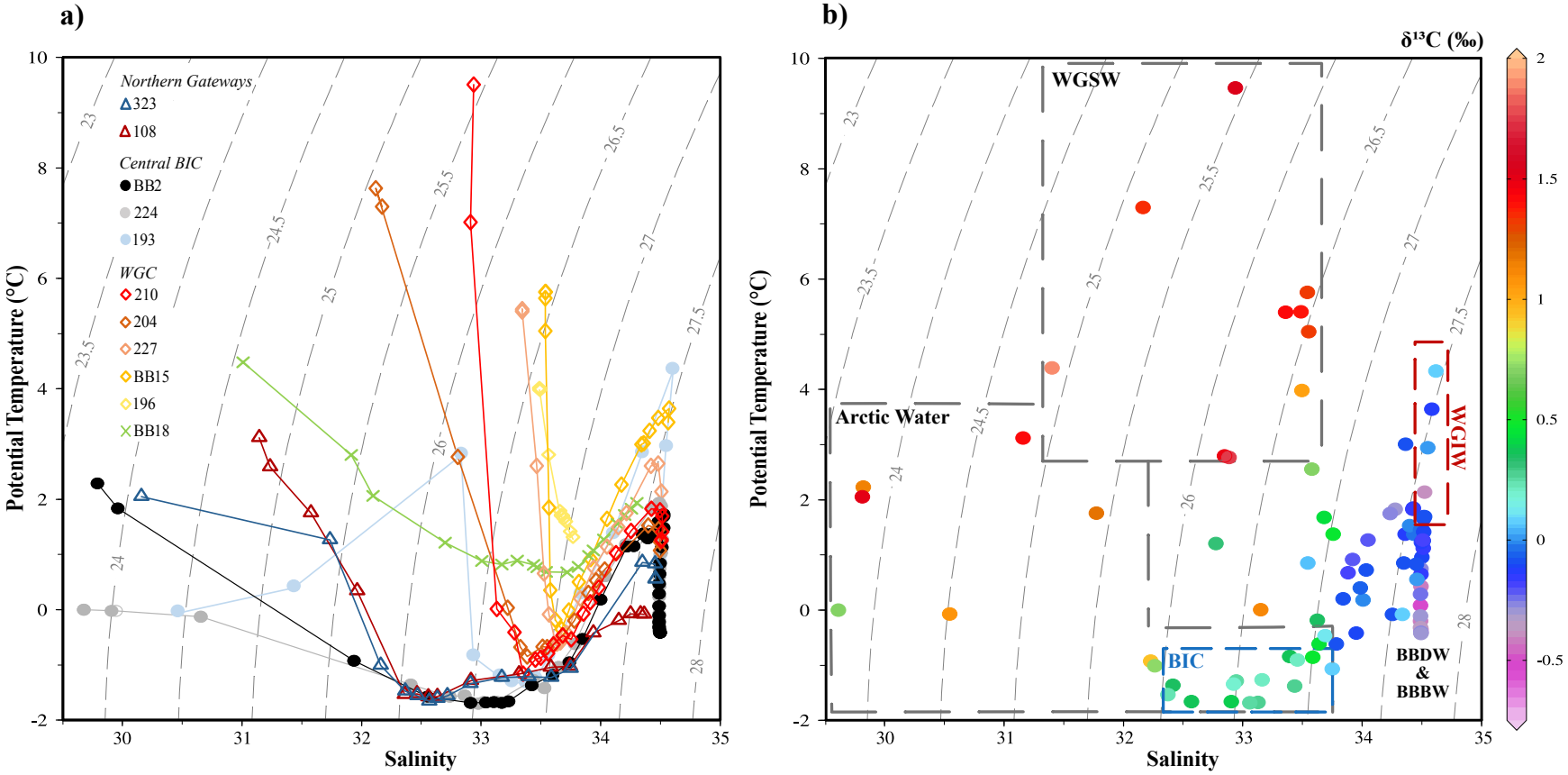

Figure 3. Potential temperature-salinity diagram with DIC $\delta^{13}C$ values throughout Baffin Bay. a) Bottle salinity and potential temperature values plotted for each collected station. Different sampled stations (Figure 1) indicated by legend; Baffin Island Current (circles), Western Greenland Current (diamonds), Northern gateways (triangles). Dashed grey lines represent potential density contours. **b)** Potential temperature versus bottle salinity labelled with DIC $\delta^{13}C$. Dashed boxes indicate designated currents and water masses; Arctic water, western Greenland shelf water (WGSW), Baffin island current (BIC), West Greenland Irminger water (WGIW), and Baffin Bay deep and bottom water (BBDW; BBBW).

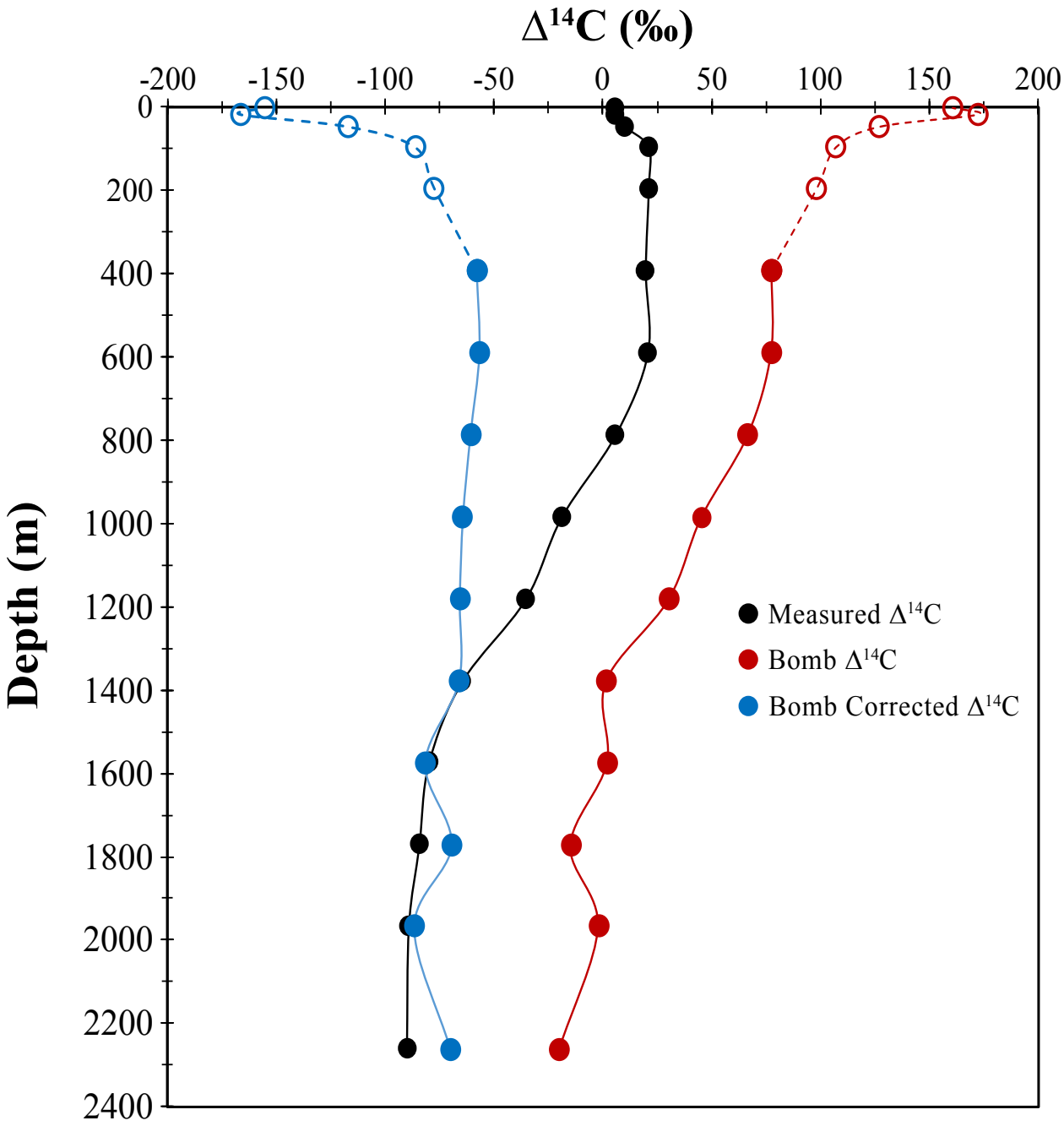

Figure 4. Calculated bomb $\Delta^{14}C$ and natural $\Delta^{14}C$ values for Baffin Bay deep water. Measured DIC $\Delta^{14}C$ values for deepest station collected in Baffin Bay, BB2 (Figure 1). Calculated $\Delta^{14}C_{bomb}$ and $\Delta^{14}C_{bomb\ corr}$ values derived using the Potential Alkalinity (P_{alk}) method (Rubin and Key, 2002) method (*see section 2.5*). Dashed lines and open circle indicate overestimated natural and bomb $\Delta^{14}C$ values above 800m.

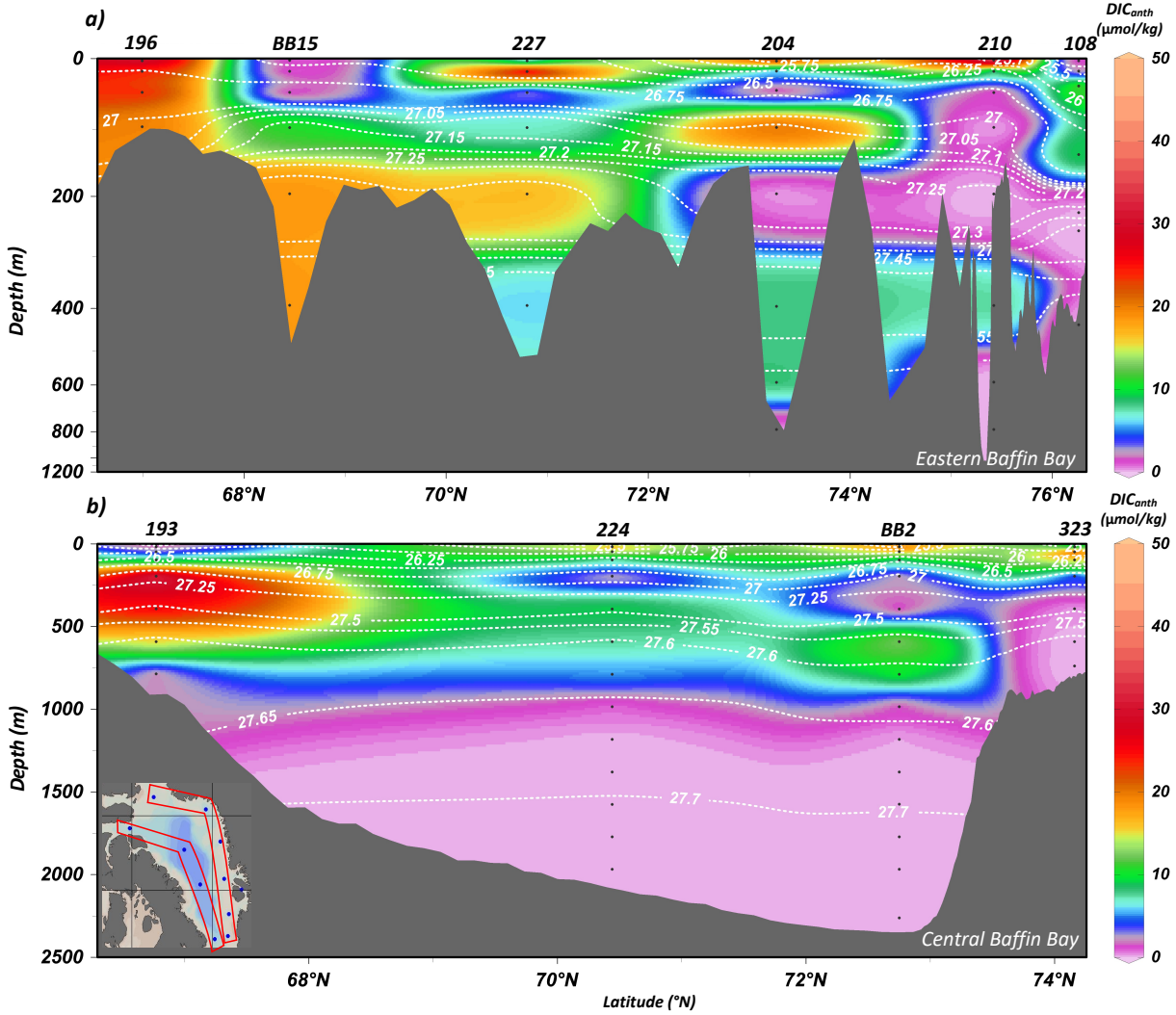

Figure 5. Calculated DIC_{anth} concentrations found throughout central and Eastern Baffin Bay. Distributions of DIC_{anth} concentrations plotted from two transects along **a)** the east coast of Greenland and **b)** central Baffin Bay, as indicated by the inset on b). DIC_{anth} concentrations calculated based on methods by (Lee et al.,2003). DIC_{anth} values <5µmol kg^{-1} are assumed to contain zero DIC_{anth} (See section 2.5). Sample depths and locations are indicated by black dots, with station names labelled at the top of the plots. Dashed white contours are potential density (σ_θ in kg m^{-3}) isopycnals.

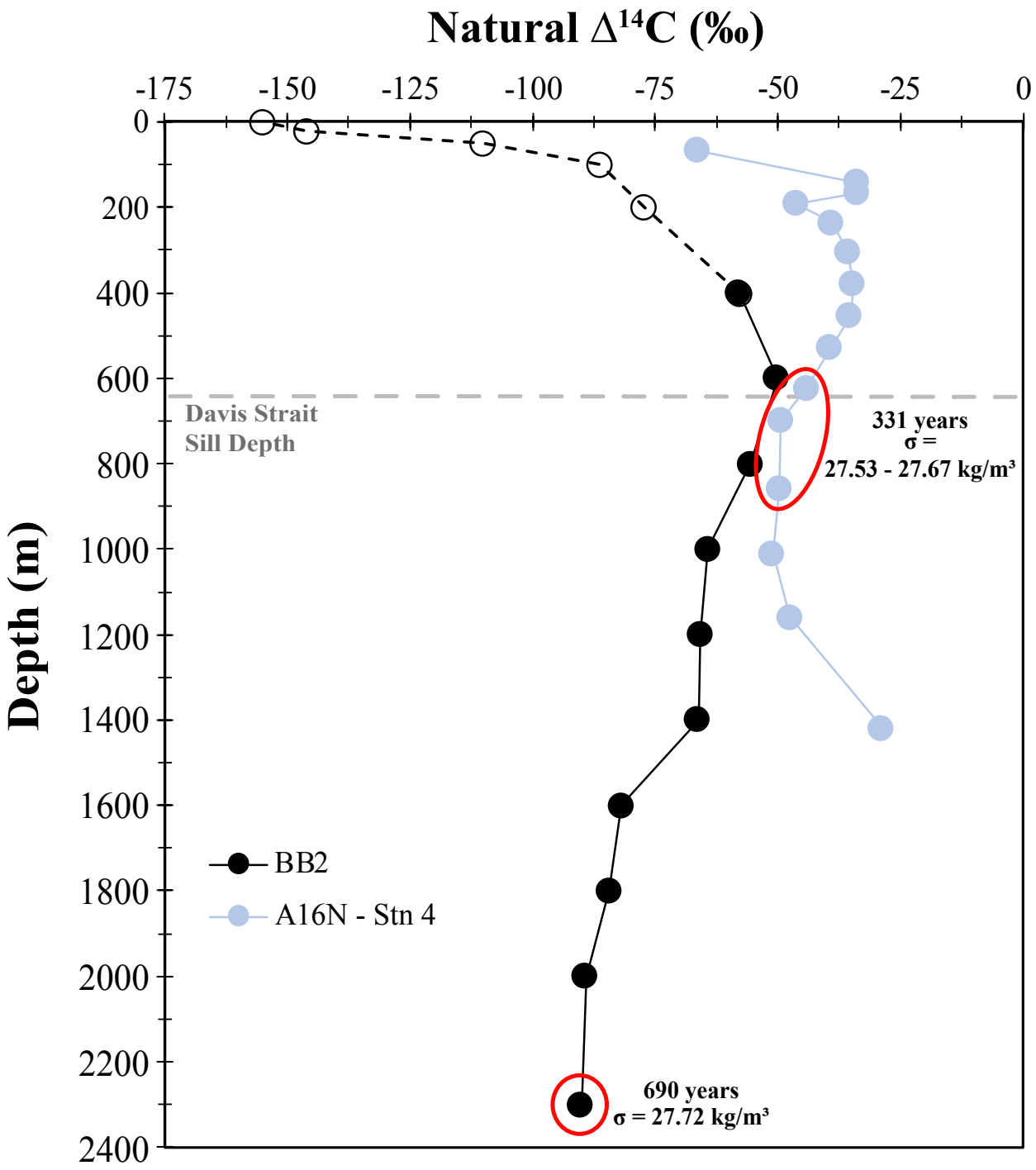

Figure 6. DIC $\Delta^{14}C_{natural}$ depth profiles, corrected for both $\Delta^{14}C_{bomb}$ and DIC_{anth} contributions for Station BB2 and A16N. DIC $\Delta^{14}C_{natural}$ values from A16N (Station 4; 62.75°N, -20.00°W) were corrected for DIC_{anth} and $\Delta^{14}C_{bomb}$. Apparent ^{14}C-ages are calculated based on $\Delta^{14}C_{natural}$ values (*see section 2.4*) for depths with potential densities close to BBBW values (θ_σ = 27.7 kg m^{-3}). Dashed horizontal grey line indicated depth of the Davis Strait sill, at 640m. Dashed and open circles for BB2 profile indicate unconstrained $\Delta^{14}C_{natural}$ values based on limitation of the P_{alk} proxy. Red circles indicate depths at which apparent ^{14}C-ages were calculated.

10. Conclusion

The Arctic Ocean is a region undergoing rapid climate and ecological change. The Arctic Ocean carbon cycle is being impacted by anthropogenic climate change. However, more measurements are needed to constrain the impact of global climate change on Arctic biogeochemical cycles. The Arctic Ocean is covered by sea-ice most of the year. This inhibits air-sea gas exchange and as a result the Arctic Ocean has low aqueous CO_2. Global climate change, warming temperatures and diminished sea ice has resulted in the Arctic Ocean becoming a sink for atmospheric CO_2, with enhanced CO_2 uptake by ~28% per decade (Bates et al., 2006). An increase in anthropogenic CO_2 has also been observed throughout the Arctic Ocean, with an estimated accumulation of 44 ± 53 Tg C yr^{-1} (MacGilchrist et al., 2014). Increased delivery of terrestrial carbon via rivers has also been observed. It has been estimated 43 Tg C/yr of DIC, 33 Tg C/yr of dissolved organic carbon (DOC), and 6 Tg C/yr of particulate organic carbon (POC) are delivered to the Arctic Ocean (McGuire et al., 2009). The Arctic carbon cycle thus has the potential to influence both local and global climate systems. However, the future response of the Arctic carbon cycle remains highly uncertain (McGuire et al., 2009). An overarching goal of this thesis, is that the marine DIC $\delta^{13}C$ and $\Delta^{14}C$ measurements provided here will 'add a piece to the puzzle' and help scientists further constrain how the Arctic will respond to climate change.

DIC $\delta^{13}C$ and $\Delta^{14}C$ isotopic measurements were made throughout Baffin Bay aboard the CCGS *Amundsen* in summer 2019. DIC $\delta^{13}C$ values had a wide range (~2.60‰), and were largely predicted by water mass density in Baffin Bay, indicative of unique DIC $\delta^{13}C$ source endmembers. DIC $\Delta^{14}C$ values also had a large range (~120.0‰) from surface to deep Baffin Bay, suggesting slow rates of deep water ventilation. We used several proxies to isolate the influence of atmospheric $\Delta^{14}C_{bomb}$ (P_{alk} proxy) and fossil anthropogenic C (DIC_{anth}; ΔC^* proxy) from natural DIC $\Delta^{14}C$. We found the P_{alk} proxy over estimated $\Delta^{14}C_{bomb}$ in Arctic waters shallower than 400m due to large ranges in surface total alkalinity and salinity versus the Atlantic Ocean (<60°N/S), for which this proxy was developed. Below 1000m the P_{alk} proxy suggested reliably low $\Delta^{14}C_{bomb}$ contributions, and no $\Delta^{14}C_{bomb}$ was estimated below 1400m. The ΔC^* method (Lee et al., 2003) was used to estimate the amount of DIC_{anth}. Unlike the P_{alk} method, the ΔC^* proxy underestimated DIC_{anth} contributions in the surface (<20m), resulting in some negative apparent DIC_{anth} concentrations. We observed a bimodal distribution of DIC_{anth} in Baffin Bay, with rich DIC_{anth}

waters entering Davis Strait while low DIC_{anth} concentrations were present in Northern Baffin Bay. Below 1000m, no DIC_{anth} is observed throughout Baffin Bay. Since no $\Delta^{14}C_{bomb}$ or DIC_{anth} are discernably present BBBW, we used our measured DIC $\Delta^{14}C$ values to estimate a deep water residence time between 360-690 years.

Baffin Bay plays an important role in Atlantic meridional overturning circulation (AMOC) through the export of cold water to the Labrador Sea, a key region of NADW formation which drives global thermohaline overturning circulation (Zweng and Münchow, 2006). Increases in freshwater export into the northern Labrador Sea can result in increased stratification and decreased deep water formation (Goosse et al., 1997). The strength of the BIC and WGC can be similarly be impacted by the North-Atlantic Oscillation (NAO) modes. A positive phase represents a more depressed Icelandic Low, resulting in drier and colder winter conditions over Greenland and Northern Canada. Negative phases are associated with weaker southerly winter conditions (Hurrell and Deser, 2009). During positive NOA phases, the BIC is fresher and colder while the WGC is warmer and saltier in comparison to the negative phase. This results in a stronger cyclonic circulation within Baffin Bay during positive NAO, but also a clear impact on AMOC (Münchow et al., 2015). With increased carbon uptake into the Arctic Ocean due to climate change, Baffin Bay has the potential to export carbon rich waters to both Atlantic Intermediate and Deep Water. In this way, Baffin Bay provides a carbon teleconnection for the global oceans via AMOC. With a residence time of 360-690 years, Baffin Bay has the potential to store DIC over centuries and lock away excess anthropogenic carbon. My work therefore suggests Baffin Bay as a key player in the Arctic marine carbon cycle.

11. References

Alkire, M. B., Falkner, K. K., Boyd, T., and Macdonald, R. W. (2010). Sea ice melt and meteoric water distributions in Nares Strait, Baffin Bay, and the Canadian Arctic Archipelago. *J Mar Res* 68, 767–798. doi:10.1357/002224010796673867.

Anderson, L. A., & Sarmiento, J. L. 1994. Redfield ratios of remineralization determined by nutrient data analysis. *Global biogeochemical cycles*, *8*(1), 65-80. https://doi.org/10.1029/93gb03318

Aminot, A. and Kérouel, R.: Dosage automatique des nutriments dans les eaux marines: méthodes en flux continu, edited by: IFREMER, Méthodes d'analyse en milieu marin, 188 pp., 2007

Azetsu-Scott, K., Petrie, B., Yeats, P., and Lee, C. (2012). Composition and fluxes of freshwater through Davis Strait using multiple chemical tracers. *J Geophys Res Oceans 1978 2012* 117, n/a-n/a. doi:10.1029/2012jc008172.

Arctic Monitoring & Assessment Programme Arctic Climate Change Update (2021). *Key Trends and Impacts - Summary for Policy-Makers*. Arctic Council Secretariat, Summary Report. https://oaarchive.arctic-council.org/handle/11374/2621

Bacon, S., Reverdin, G., Rigor, I. G., and Snaith, H. M. (2002). A freshwater jet on the east Greenland shelf. *J Geophys Res Oceans 1978 2012* 107, 5-1-5–16. doi:10.1029/2001jc000935.

Bailey, W. B. (1956). On the Origin of Deep Baffin Bay Water. *J Fish Board Can* 13, 303–308. doi:10.1139/f56-020.

Bamber, J., Broeke, M. den, Ettema, J., Lenaerts, J., and Rignot, E. (2012). Recent large increases in freshwater fluxes from Greenland into the North Atlantic. *Geophys Res Lett* 39, n/a-n/a. doi:10.1029/2012gl052552.

Bates, N. R., Moran, S. B., Hansell, D. A., and Mathis, J. T. (2006). An increasing CO_2 sink in the Arctic Ocean due to sea-ice loss. *Geophys Res Lett* 33. doi:10.1029/2006gl027028.

Bauch, D., Polyak, L., and Ortiz, J. D. (2015). A baseline for the vertical distribution of the stable carbon isotopes of dissolved inorganic carbon (δ^{13}DIC) in the Arctic Ocean. *Arktos* 1, 15. doi:10.1007/s41063-015-0001-0.

Bourke, R. H., Addison, V. G., and Paquette, R. G. (1989). Oceanography of Nares Strait and northern Baffin Bay in 1986 with emphasis on deep and bottom water formation. *J Geophys Res* 94, 8289. doi:10.1029/jc094ic06p08289.

Bourke, R. H., and Paquette, R. G. (1991). Formation of Baffin Bay Bottom and Deep Waters. *Elsev Oceanogr Serie* 57, 135–155. doi:10.1016/s0422-9894(08)70065-5.

Broecker, W. S., Gerard, R., Ewing, M., and Heezen, B. C. (1960). Natural radiocarbon in the Atlantic Ocean. *J Geophys Res* 65, 2903–2931. doi:10.1029/jz065i009p02903.

Brown, T. A., and Reimer, R. W. (2004). Discussion: Reporting and Calibration of Post-Bomb ^{14}C Data. *Radiocarbon* 46, 1299–1304. doi:10.1017/s0033822200033154.

Bullister, J. and Barigner, M. 2020. Bottle data from Cruise 33RO20130803, exchange version. Accessed from CCHDO https://cchdo.ucsd.edu/cruise/33RO20130803. Access date 2021-09-15.

Carter, B. R., Feely, R. A., Wanninkhof, R., Kouketsu, S., Sonnerup, R. E., Pardo, P. C., et al. (2019). Pacific Anthropogenic Carbon Between 1991 and 2017. *Global Biogeochem Cy* 33, 597–617. doi:10.1029/2018gb006154.

Chen, G.-T., and Millero, F. J. (1979). Gradual increase of oceanic CO_2. *Nature* 277, 205–206. doi:10.1038/277205a0.

Collin, A. E. (1965). Report 65–5, 9 pp., Bedford Institute of Oceanography Report, Dartmouth, NS

Cuny, J., Rhines, P. B., and Kwok, R. (2005). Davis Strait volume, freshwater and heat fluxes. *Deep Sea Res Part Oceanogr Res Pap* 52, 519–542. doi:10.1016/j.dsr.2004.10.006.

Cuny, J., Rhines, P. B., Niiler, P. P., and Bacon, S. (2002). Labrador Sea Boundary Currents and the Fate of the Irminger Sea Water. *J Phys Oceanogr* 32, 627–647. doi:10.1175/1520-0485(2002)032<0627:lsbcat>2.0.co;2.

Curry, B., Lee, C. M., and Petrie, B. (2011). Volume, Freshwater, and Heat Fluxes through Davis Strait, 2004–05*. *J Phys Oceanogr* 41, 429–436. doi:10.1175/2010jpo4536.1.

Curry, B., Lee, C. M., Petrie, B., Moritz, R. E., and Kwok, R. (2014). Multiyear Volume, Liquid Freshwater, and Sea Ice Transports through Davis Strait, 2004–10*. *J Phys Oceanogr* 44, 1244–1266. doi:10.1175/jpo-d-13-0177.1.

Dickson, A. G., Sabine, C. L., & Christian, J. R. (2007). *Guide to best practices for ocean CO2 measurements*. North Pacific Marine Science Organization.

Druffel, E. R. M., Griffin, S., Glynn, C. S., Benner, R., and Walker, B. D. (2017). Radiocarbon in dissolved organic and inorganic carbon of the Arctic Ocean. *Geophys Res Lett* 44, 2369–2376. doi:10.1002/2016gl072138.

Dutta, K. (2008). Marine ^{14}C reservoir age and Suess effect in the Indian Ocean. *Earth Science India*, *1*.

Emerson, S., and Hedges, J. (2008). Chemical Oceanography and the Marine Carbon Cycle. ix–ix. doi:10.1017/cbo9780511793202.001.

Fissel, D. B., Lemon, D. D., and Birch, J. R. (1982). Major Features of the Summer Near-Surface Circulation of Western Baffin Bay, 1978 and 1979. *Arctic* 35. doi:10.14430/arctic2318.

Fox, A., Walker, B. (in review). Sources and cycling of particulate organic matter in Baffin Bay: a combined $\delta^{13}C$ and $\Delta^{14}C$ approach. *Frontiers in Marine Science.*

Gao, P., Xu, X., Zhou, L., Pack, M. A., Griffin, S., Santos, G. M., et al. (2014). Rapid sample preparation of dissolved inorganic carbon in natural waters using a headspace-extraction approach for radiocarbon analysis by accelerator mass spectrometry. *Limnology Oceanogr Methods* 12, 174–190. doi:10.4319/lom.2014.12.174.

Goosse, H., Fichefet, T., and Campin, J. -M. (1997). The effects of the water flow through the Canadian Archipelago in a global ice-ocean model. *Geophys Res Lett* 24, 1507–1510. doi:10.1029/97gl01352.

Griffith, D. R., McNichol, A. P., Xu, L., McLaughlin, F. A., Macdonald, R. W., Brown, K. A., et al. (2012). Carbon dynamics in the western Arctic Ocean: insights from full-depth carbon isotope profiles of DIC, DOC, and POC. *Biogeosciences* 9, 1217–1224. doi:10.5194/bg-9-1217-2012.

Gruber, N., Clement, D., Carter, B. R., Feely, R. A., van Heuven, S., Hoppema, M., ... & Wanninkhof, R. (2018, December). New observational constraints on the global ocean uptake of anthropogenic CO2. In *OCB Ocean Carbon Uptake in CMIP6 Models Synthesis and Intercomparison Workshop*.

Guilderson, T. P., Caldeira, K., and Duffy, P. B. (2000). Radiocarbon as a diagnostic tracer in ocean and carbon cycle modeling. *Global Biogeochem Cy* 14, 887–902. doi:10.1029/1999gb001192.

Hamilton, J., and Wu, Y. (2013). Synopsis and trends in the physical environment of Baffin Bay and Davis Strait. *Ocean and Ecosystem Sciences Division, Maritimes Region, Fisheries and Oceans Canada*.

Heinze, C. (2014). The Role of the Ocean Carbon Cycle in Climate Change. *Eur Rev* 22, 97–105. doi:10.1017/s1062798713000665.

Hoppema, M., Roether, W., Bellerby, R. G. J., and Baar, H. J. W. de (2001). Direct measurements reveal insignificant storage of anthropogenic CO_2 in the Abyssal Weddell Sea. *Geophys Res Lett* 28, 1747–1750. doi:10.1029/2000gl012443.

Humphreys, M. P., Greatrix, F. M., Tynan, E., Achterberg, E. P., Griffiths, A. M., Fry, C. H., et al. (2016). Stable carbon isotopes of dissolved inorganic carbon for a zonal transect across the subpolar North Atlantic Ocean in summer 2014. *Earth Syst Sci Data* 8, 221–233. doi:10.5194/essd-8-221-2016.

Hurrell, J. W., and Deser, C. (2009). North Atlantic climate variability: The role of the North Atlantic Oscillation. *J Marine Syst* 78, 28–41. doi:10.1016/j.jmarsys.2008.11.026.

Jiang, Z., Tyrrell, T., Hydes, D. J., Dai, M., and Hartman, S. E. (2014). Variability of alkalinity and the alkalinity-salinity relationship in the tropical and subtropical surface ocean. *Global Biogeochem Cy* 28, 729–742. doi:10.1002/2013gb004678.

Johnson, K. M., Wills, K. D., Butler, D. B., Johnson, W. K., & Wong, C. S. (1993). Coulometric total carbon dioxide analysis for marine studies: maximizing the performance of an automated gas extraction system and coulometric detector. *Marine Chemistry*, *44*(2-4), 167-187. https://doi.org/10.1016/0304-4203(93)90201-x

Körtzinger, A., Quay, P. D., & Sonnerup, R. E. (2003). Relationship between anthropogenic CO_2 and the ^{13}C Suess effect in the North Atlantic Ocean. *Global Biogeochemical Cycles*, *17*(1), 5-1.

Krawczyk, D. W., Kryk, A., Juggins, S., Burmeister, A., Pearce, C., Seidenkrantz, M.-S., et al. (2021). Spatio-temporal changes in ocean conditions and primary production in Baffin Bay and the Labrador Sea. *Palaeogeogr Palaeoclim Palaeoecol* 563, 110175. doi:10.1016/j.palaeo.2020.110175.

Kroopnick, P. M. (1985). The distribution of 13C of ΣCO2 in the world oceans. *Deep Sea Res Part Oceanogr Res Pap* 32, 57–84. doi:10.1016/0198-0149(85)90017-2. https://doi.org/10.1016/0198-0149(85)90017-2.

Lee, K., Choi, S. -D., Park, G. -H., Wanninkhof, R., Peng, T. -H., Key, R. M., et al. (2003). An updated anthropogenic CO_2 inventory in the Atlantic Ocean. *Global Biogeochem Cy* 17, n/a-n/a. doi:10.1029/2003gb002067.

Lehmann, N., Kienast, M., Granger, J., Bourbonnais, A., Altabet, M. A., and Tremblay, J. -É (2019). Remote Western Arctic Nutrients Fuel Remineralization in Deep Baffin Bay. *Global Biogeochem Cy* 33, 649–667. doi:10.1029/2018gb006134.

Lobb, J. (2004). On Arctic and Atlantic halocline interactions in Baffin Bay. Doctoral Thesis, University of Victoria, Victoria, British Columbia

MacGilchrist, G. A., Garabato, A. C. N., Tsubouchi, T., Bacon, S., Torres-Valdés, S., and Azetsu-Scott, K. (2014). The Arctic Ocean carbon sink. *Deep Sea Res Part Oceanogr Res Pap* 86, 39–55. doi:10.1016/j.dsr.2014.01.002.

Mackenzie, Fred T., and Abraham Lerman. "Isotopic Fractionation of Carbon: Inorganic and Biological Processes." *Carbon in the Geobiosphere—Earth's Outer Shell—*. Springer, Dordrecht, 2006. 165-191, https://doi.org/10.1007/s10498-007-9016-x

Mahadevan, A. (2001). An analysis of bomb radiocarbon trends in the Pacific. *Mar Chem* 73, 273–290. doi:10.1016/s0304-4203(00)00113-4.

McGuire, A. D., Anderson, L. G., Christensen, T. R., Dallimore, S., Guo, L., Hayes, D. J., et al. (2009). Sensitivity of the carbon cycle in the Arctic to climate change. *Ecol Monogr* 79, 523–555. doi:10.1890/08-2025.1.

Melling, H., et al. (2008), Chapter 9. Fresh-water fluxes via Pacific and Arctic Outflows across the Canadian polar shelf. In Arctic-Subarctic Ocean Fluxes: Defining the role of the Northern Seas in Climate. editted by R. R. Dickson, J. Meinke, and P. Rhines, Springer Verlag Published. https://doi.org/10.1007/978-1-4020-6774-7_10.

Melling, H., Gratton, Y., and Ingram, G. (2010). Ocean circulation within the North Water polynya of Baffin Bay. *Atmos Ocean* 39, 301–325. doi:10.1080/07055900.2001.9649683.

Min, C., Yang, Q., Mu, L., Kauker, F., and Ricker, R. (2020). Multi-model based estimation of sea ice volume variations in the Baffin Bay. *Cryosphere Discuss* 2020, 1–19. doi:10.5194/tc-2020-177.

Mol, J. (2017). The exchange of inorganic carbon on the Canadian Beaufort Shelf, https://doi.org/10.5194/bg-2017-318-rc3

Moreau, S., Vancoppenolle, M., Bopp, L., Aumont, O., Madec, G., Delille, B., ... & Miller, L. A. (2016). Assessment of the sea-ice carbon pump: Insights from a three-dimensional ocean-sea-ice biogeochemical model (NEMO-LIM-PISCES) Assessment of the sea-ice carbon pump. *Elementa: science of the anthropocene*, *4*, https://doi.org/10.12952/journal.elementa.000122

Morée, A. L., Schwinger, J., and Heinze, C. (2018). Southern Ocean controls of the vertical marine $\delta^{13}C$ gradient – a modelling study. *Biogeosciences Discuss*, 1–24. doi:10.5194/bg-2018-52.

Muench, R. D. (1970). The physical oceanography of the northern Baffin Bay region. Ph.D. thesis, University of Washington, Seattle,USA.

Münchow, A., Falkner, K. K., and Melling, H. (2015). Baffin Island and West Greenland Current Systems in northern Baffin Bay. *Prog Oceanogr* 132, 305–317. doi:10.1016/j.pocean.2014.04.001.

Münchow, A., and Melling, H. (2008). Ocean current observations from Nares Strait to the west of Greenland: Interannual to tidal variability and forcing. *J Mar Res* 66, 801–833. doi:10.1357/002224008788064612.

Murphy, R. C., Sverdrup, H. U., Johnson, M. W., and Fleming, R. H. (1944). The Oceans: Their Physics, Chemistry, and General Biology. *Geogr Rev* 34, 170. doi:10.2307/210609.

Myers, P. G., Donnelly, C., and Ribergaard, M. H. (2009). Structure and variability of the West Greenland Current in Summer derived from 6 repeat standard sections. *Prog Oceanogr* 80, 93–112. doi:10.1016/j.pocean.2008.12.003.

Naegler, T., and Levin, I. (2006). Closing the global radiocarbon budget 1945–2005. *J Geophys Res Atmospheres 1984 2012* 111. doi:10.1029/2005jd006758.

Newton, R., and Bottrell, S. (2007). Stable isotopes of carbon and sulphur as indicators of environmental change: past and present. *J Geol Soc London* 164, 691–708. doi:10.1144/0016-76492006-101.

Olack, G. A., Colman, A. S., Pfister, C. A., and Wootton, J. T. (2018). Seawater DIC analysis: The effects of blanks and long-term storage on measurements of concentration and stable isotope composition: The analysis of seawater carbon. *Limnology Oceanogr Methods* 16, 160–179. doi:10.1002/lom3.10235.

Olsen, A., Anderson, L. G., & Heinze, C. (2015). Arctic carbon cycle: Patterns, impacts and possible changes. In *The New Arctic* (pp. 95-115). Springer, Cham. https://doi.org/10.1007/978-3-319-17602-4_8

Östlund, H. G., Possnert, G., and Swift, J. H. (1987). Ventilation rate of the deep Arctic Ocean from carbon 14 data. *J Geophys Res Oceans* 92, 3769–3777. doi:10.1029/jc092ic04p03769.

Peterson, I.K. and R. Pettipas (2013), Trends in Air Temperature and Sea Ice in the Atlantic Basin and Adjoining Areas. Can. Tech. Rep. Hydrogr. Ocean Sci. xxx:v + 58 p. Under review.

Poisson, A., and Chen, C.-T. A. (1987). Why is there little anthropogenic CO_2 in the Antarttic bottom water? *Deep Sea Res Part Oceanogr Res Pap* 34, 1255–1275. doi:10.1016/0198-0149(87)90075-6.

Quay, P., Sonnerup, R., Westby, T., Stutsman, J., and McNichol, A. (2003). Changes in the $^{13}C/^{12}C$ of dissolved inorganic carbon in the ocean as a tracer of anthropogenic CO_2 uptake. *Global Biogeochem Cy* 17, 4-1-4–20. doi:10.1029/2001gb001817.

Rignot, E., Velicogna, I., Broeke, M. R. van den, Monaghan, A., and Lenaerts, J. T. M. (2011). Acceleration of the contribution of the Greenland and Antarctic ice sheets to sea level rise. *Geophys Res Lett* 38, n/a-n/a. doi:10.1029/2011gl046583.

Rodgers, K. B., Schrag, D. P., Cane, M. A., and Naik, N. H. (2000). The bomb 14C transient in the Pacific Ocean. *J Geophys Res Oceans* 105, 8489–8512. doi:10.1029/1999jc900228.

Rubin, S. I., and Key, R. M. (2002). Separating natural and bomb-produced radiocarbon in the ocean: The potential alkalinity method. *Global Biogeochem Cy* 16, 52-1-52–19. doi:10.1029/2001gb001432.

Rudels, B., Jones, E. P., Schauer, U., and Eriksson, P. (2004). Atlantic sources of the Arctic Ocean surface and halocline waters. *Polar Res* 23, 181–208. doi:10.1111/j.1751-8369.2004.tb00007.x.

Rykova, T., Straneo, F., Lilly, J. M., and Yashayaev, I. (2009). Irminger Current Anticyclones in the Labrador Sea observed in the hydrographic record, 1990–2004. *J Mar Res* 67, 361–384. doi:10.1357/002224009789954739.

Rysgaard, S., Glud, R. N., Sejr, M. K., Bendtsen, J., and Christensen, P. B. (2007). Inorganic carbon transport during sea ice growth and decay: A carbon pump in polar seas. *J Geophys Res Oceans 1978 2012* 112. doi:10.1029/2006jc003572.

Sabine, C. L., Feely, R. A., Gruber, N., Key, R. M., Lee, K., Bullister, J. L., et al. (2004). The Oceanic Sink for Anthropogenic CO_2. *Science* 305, 367–371. doi:10.1126/science.1097403.

Sadler, H. E. (1976). Water, Heat, and Salt Transports through Nares Strait, Ellesmere Island. *J Fish Board Can* 33, 2286–2295. doi:10.1139/f76-275.

Sasgen, I., Wouters, B., Gardner, A. S., King, M. D., Tedesco, M., Landerer, F. W., et al. (2020). Return to rapid ice loss in Greenland and record loss in 2019 detected by the GRACE-FO satellites. *Commun Earth Environ* 1, 8. doi:10.1038/s43247-020-0010-1.

Serreze, M. C., Barrett, A. P., Slater, A. G., Woodgate, R. A., Aagaard, K., Lammers, R. B., et al. (2006). The large-scale freshwater cycle of the Arctic. *J Geophys Res Oceans 1978 2012* 111. doi:10.1029/2005jc003424.

Shadwick, E. H., Thomas, H., Chierici, M., Else, B., Fransson, A., Michel, C., et al. (2011). Seasonal variability of the inorganic carbon system in the Amundsen Gulf region of the southeastern Beaufort Sea. *Limnol Oceanogr* 56, 303–322. doi:10.4319/lo.2011.56.1.0303.

Sharp, Z. (2007). Principles of stable isotope geochemistry. *Choice Rev Online* 44, 44-6251-44–6251. doi:10.5860/choice.44-6251.

Stuiver, M., and Polach, H. A. (1977). Discussion Reporting of ^{14}C Data. *Radiocarbon* 19, 355–363. doi:10.1017/s0033822200003672.

Stuiver, M., Quay, P. D., and Ostlund, H. G. (1983). Abyssal Water Carbon-14 Distribution and the Age of the World Oceans. *Science* 219, 849–851. doi:10.1126/science.219.4586.849.

Suess, Hans E. "Natural radiocarbon and the rate of exchange of carbon dioxide between the atmosphere and the sea." *Nuclear processes in geologic settings* 43 (1953): 52-56.

Sutherland, D. A., and Pickart, R. S. (2008). The East Greenland Coastal Current: Structure, variability, and forcing. *Prog Oceanogr* 78, 58–77. doi:10.1016/j.pocean.2007.09.006.

Sverdrup, H. V., Johnson, M. W., & Fleming, R. H. (1942). The ocean, their physics, chemistry and general biology. Englewood Cliffs, NJ, USA: Prentice-Hall, pp. 1087, https://doi.org/10.2307/520072

Sweeney, C., Gloor, E., Jacobson, A. R., Key, R. M., McKinley, G., Sarmiento, J. L., et al. (2007). Constraining global air-sea gas exchange for CO_2 with recent bomb ^{14}C measurements. *Global Biogeochem Cy* 21, n/a-n/a. doi:10.1029/2006gb002784.

Takahashi, T., Broecker, W. S., & Bainbridge, A. E. (1981). The alkalinity and total carbon dioxide concentration in the world oceans. *Carbon cycle modelling, SCOPE*, *16*(3078), 271-286.

Tan, F. C., and Strain, P. M. (1980). The distribution of sea ice meltwater in the eastern Canadian Arctic. *J Geophys Res Oceans* 85, 1925–1932. doi:10.1029/jc085ic04p01925.

Tang, C. C. L., Ross, C. K., Yao, T., Petrie, B., DeTracey, B. M., and Dunlap, E. (2004). The circulation, water masses and sea-ice of Baffin Bay. *Prog Oceanogr* 63, 183–228. doi:10.1016/j.pocean.2004.09.005.

Tjiputra, J. F., Assmann, K., and Heinze, C. (2010). Anthropogenic carbon dynamics in the changing ocean. *Ocean Sci* 6, 605–614. doi:10.5194/os-6-605-2010.

Top, Z., Clarke, W. B., Eismont, W. C., & Jones, E. P. 1980. Radiogenic helium in Baffin Bay bottom water. Journal of Marine Research,38(3), 435–452, https://doi.org/10.4095/119621

Wallace, D. W. R. 1985. A study of the ventilation of Arctic water using chlorofluoromethanes as tracers. Halifax NS, Canada: Dalhousie University.

Wareham, V. E. (2009). Updates on deep-sea coral distributions in the Newfoundland and Labrador and Arctic Regions, Northwest Atlantic. *The ecology of deep-sea corals of Newfoundland and Labrador water: biogeography, life history, biogeochemistry, and relation to fishes. Can. Tech. Rep. Fish. Aquat. Sci*, *2830*, 4-22.

Xu, X., Trumbore, S. E., Zheng, S., Southon, J. R., McDuffee, K. E., Luttgen, M., et al. (2007). Modifying a sealed tube zinc reduction method for preparation of AMS graphite targets: Reducing background and attaining high precision. *Nucl Instruments Methods Phys Res Sect B Beam Interactions Mater Atoms* 259, 320–329. doi:10.1016/j.nimb.2007.01.175.

Zhang, J., Quay, P. D., and Wilbur, D. O. (1995). Carbon isotope fractionation during gas-water exchange and dissolution of CO_2. *Geochim Cosmochim Ac* 59, 107–114. doi:10.1016/0016-7037(95)91550-d.

Zhang X., Flato G., Kirchmeier-Yong M., Vincent L., Wan H., Wang X., Rong R., Fyfe J., Li G. and Kharin V. 2019. Changes in Temperature and Precipitation Across Canada. In Canada's Changing Climate Report (eds. E. Bush and D. S. Lemmen). Ottawa, Ontario. pp. 112–193, https://doi.org/10.4095/327811

Zweng, M. M., and Münchow, A. (2006). Warming and freshening of Baffin Bay, 1916–2003. *J Geophys Res Oceans 1978 2012* 111. doi:10.1029/2005jc003093

Appendix A: Extended data tables of measured and derived parameters

Table A1: Summary of measured data from the CCGS *Amundsen* in July 2019. Temperature, potential temperature, salinity, potential density, and dissolved oxygen data are from sensors on the CTD rosette. Nitrate measurements were conducted at Université Laval (±1 µmol/kg). Dissolved inorganic carbon (DIC) and total alkalinity (TA) concentrations had errors of ± 7.76 µmol/kg (n = 24) and ± 14.27 µmol/kg (n = 24), respectively. DIC $\delta^{13}C$ values (‰) measured at the Jan Veizer Stable Isotope Laboratory with an external precision of ±0.1‰. Fraction modern, $\Delta^{14}C$, and ^{14}C ages measured at the Keck Carbon Cycle AMS facility at the University of California. True DIC $\Delta^{14}C$ sample bottle replicates indicated by (†).

Station	Latitude °N	Longitude °W	Depth m	Temp °C	θ °C	Salinity	σ_0 Kg/m^3	Nitrate µmol/kg	DO µmol/kg	A_T µmol/kg	DIC µmol/kg	$\delta^{13}C$ ‰	UCIAMS #	Fraction Modern	±	$\Delta^{14}C$ ‰	± ‰	^{14}C Age Years	± Years
193	66 46.18	59 20.41	787	1.00	1.03	34.50	27.64	643	194	2275	2210	-0.12	236301	1.0004	0.0012	-7.9	1.2	0	15
193	66 46.18	59 20.41	592	1.48	1.46	34.50	27.61	628	207	2261	2206	-0.13	236302	1.0135	0.0013	5.1	1.3	Modern	
193†	66 46.18	59 20.41	393	2.97	2.75	34.55	27.53	557	239	2277	2180	0.01	236303	1.0270	0.0013	18.5	1.3	Modern	
													236304	1.0238	0.0013	15.3	1.3	Modern	
193	66 46.18	59 20.41	196	4.35	4.65	34.61	27.44	499	264	2279	2155	0.07	236305	1.0257	0.0013	17.2	1.3	Modern	
193	66 46.18	59 20.41	98	-0.85	-0.81	33.57	26.99	227	316	2234	2133	0.47	236306	1.0291	0.0013	20.5	1.3	Modern	
193	66 46.18	59 20.41	48	-1.26	-1.35	33.16	26.67	332	285	2233	2152	0.21	236307	1.0246	0.0013	16.0	1.3	Modern	
193	66 46.18	59 20.41	18	2.80	3.29	32.83	26.17	21	349	2199	2015	1.47	236308	1.0242	0.0014	15.7	1.4	Modern	
193	66 46.18	59 20.41	3	-0.07	-0.28	30.40	24.40	9	360	2106	1979	1.06	236312	1.0161	0.0016	7.6	1.6	Modern	
196	66 59.21	56 03.57	97	1.38	1.43	33.75	27.01	220	308	2234	2119	0.46	236313	1.0290	0.0014	20.4	1.4	Modern	
196	66 59.21	56 03.57	48	1.68	1.70	33.68	26.93	180	311	2234	2114	0.43	236314	1.0255	0.0016	17.0	1.6	Modern	
196	66 59.21	56 03.57	18	2.56	3.39	33.59	26.80	79	323	2233	2081	0.70	236315	1.0314	0.0014	22.9	1.4	Modern	
196†	66 59.21	56 03.57	4	3.98	3.80	33.49	26.59	4	331	2198	2052	1.03	236316	1.0272	0.0014	18.7	1.4	Modern	
													236317	1.0285	0.0013	20.0	1.3	Modern	
BB15	68 27.08	55 53.99	394	3.67	3.65	34.57	27.48	544	246	2305	2171	-0.13	236318	1.0247	0.0015	16.2	1.5	Modern	
BB15	68 27.08	55 53.99	197	3.02	3.00	34.36	27.37	520	252	2284	2164	-0.09	236319	1.0277	0.0014	19.2	1.4	Modern	
BB15	68 27.08	55 53.99	98	0.92	0.85	33.92	27.18	436	267	2252	2158	-0.22	236320	1.0257	0.0014	17.2	1.4	Modern	
BB15	68 27.08	55 53.99	48	-0.18	-0.22	33.62	27.00	70	348	2251	2089	0.35	236321	1.0279	0.0017	19.4	1.7	Modern	
BB15	68 27.08	55 53.99	18	5.05	5.35	33.54	26.51	0	316	2259	2015	1.31	236322	1.0270	0.0016	18.5	1.6	Modern	
BB15	68 27.08	55 53.99	3	5.76	5.59	33.54	26.43	0	305	2256	2021	1.32	236323	1.0245	0.0020	15.9	2.0	Modern	
BB18	70 05.40	52 44.40	396	1.85	1.82	34.26	27.39	549	232	2284	2182	-0.30	240010	1.0247	0.0017	16.2	1.7	Modern	
BB18	70 05.40	52 44.40	196	1.28	1.29	34.03	27.24	507	250	2266	2173	-0.22	240011	1.0254	0.0016	16.9	1.6	Modern	
BB18	70 05.40	52 44.40	98	0.68	0.70	33.72	27.04	446	268	2242	2141	-0.18	240012	1.0262	0.0017	17.6	1.7	Modern	
BB18	70 05.40	52 44.40	48	0.86	0.89	33.32	26.70	349	279	2225	2114	0.05	240013	1.0301	0.0016	21.6	1.6	Modern	
BB18†	70 05.40	52 44.40	19	1.21	1.43	32.70	26.18	265	302	2192	2038	0.30	240014	1.0280	0.0016	19.4	1.6	Modern	
													240019	1.0283	0.0018	19.7	1.8	Modern	
BB18	70 05.40	52 44.40	3	4.39	NaN	31.06	24.61	0	381	2092	1814	1.90	240020	1.0266	0.0016	18.1	1.6	Modern	
227†	70 47.81	56 59.27	394	2.16	2.13	34.51	27.57	603	215	2284	2192	-0.39	237416	1.0230	0.0017	14.5	1.7	Modern	
													237417	1.0229	0.0017	14.4	1.7	Modern	
227	70 47.81	56 59.27	197	1.76	1.82	34.22	27.36	542	240	2243	2167	-0.28	237418	1.0274	0.0015	18.8	1.5	Modern	
227	70 47.81	56 59.27	98	0.21	0.32	33.83	27.15	461	265	2246	2160	-0.09	237419	1.0263	0.0016	17.7	1.6	Modern	
227	70 47.81	56 59.27	48	-0.61	-0.66	33.63	27.02	313	296	2241	2138	0.44	237420	1.0293	0.0016	20.8	1.6	Modern	

227	70 47.81	56 59.27	19	5.40	5.47	33.34	26.32	0	309	2230	2062	1.41	237421	1.0272	0.0014	18.6	1.4	Modern	
227	70 47.81	56 59.27	4	5.41	5.46	33.34	26.31	0	309	2282	2020	1.40	237422	1.0288	0.0016	20.2	1.6	Modern	
224	70 25.20	62 56.71	1969	-0.30	-0.40	34.50	27.72	857	111	2287	2276	-0.68	237436	0.9181	0.0013	-89.5	1.3	685	15
224	70 25.20	62 56.71	1773	-0.26	-0.35	34.49	27.71	841	116	2292	2270	-0.43	237437	0.9210	0.0013	-86.7	1.3	660	15
224	70 25.20	62 56.71	1576	-0.12	-0.20	34.49	27.70	816	122	2281	2263	-0.43	237438	0.9257	0.0013	-82.0	1.3	620	15
224	70 25.20	62 56.71	1380	0.15	0.08	34.49	27.69	779	136	2285	2250	-0.52	237439	0.9344	0.0015	-73.4	1.5	545	15
224	70 25.20	62 56.71	1183	0.49	0.44	34.49	27.67	711	161	2281	2230	-0.43	237440	0.9554	0.0014	-52.6	1.4	365	15
224†	70 25.20	62 56.71	986	0.80	0.75	34.49	27.65	662	186	2276	2217	-0.27	237441	0.9857	0.0015	-22.5	1.5	115	15
													237442	0.9862	0.0015	-22.0	1.5	110	15
224†	70 26.44	62 56.71	789	1.30	1.28	34.52	27.64	644	194	2276	2211	-0.11	237423	1.0013	0.0015	-7.0	1.5	Modern	
													237425	1.0046	0.0015	-3.7	1.5	Modern	
224	70 26.44	62 56.71	592	1.69	1.77	34.52	27.61	612	210	2284	2200	-0.11	237426	1.0159	0.0014	7.5	1.4	Modern	
224	70 26.44	62 56.71	394	1.87	1.84	34.43	27.53	576	224	2281	2191	-0.14	237427	1.0282	0.0015	19.6	1.5	Modern	
224	70 26.44	62 56.71	197	-0.61	-0.50	33.78	27.15	459	262	2252	2172	-0.08	237428	1.0266	0.0014	18.1	1.4	Modern	
224	70 26.44	62 56.71	98	-1.67	-1.69	33.13	26.66	335	301	2248	2155	0.26	237429	1.0238	0.0013	15.3	1.3	Modern	
224	70 26.44	62 56.71	48	-1.66	-1.66	32.90	26.47	229	322	2243	2148	0.39	237430	1.0165	0.0015	8.1	1.5	Modern	
224	70 26.44	62 56.71	19	-1.36	-1.34	32.41	26.07	180	346	2236	2133	0.34	240021	1.0162	0.0018	7.7	1.8	Modern	
224	70 26.44	62 56.71	3	0.00	NaN	29.68	23.81	3	362	2096	1962	0.69	237432	1.0172	0.0015	8.7	1.5	Modern	
BB2†	72 44.94	66 59.69	2262	-0.30	-0.42	34.50	27.72	NaN	112	2285	2279	-0.29	236333	0.9169	0.0013	-90.7	1.3	695	15
													236334	0.9184	0.0012	-89.2	1.2	685	15
BB2	72 44.94	66 59.69	1968	-0.30	-0.40	34.49	27.72	830	117	2302	2273	-0.27	236335	0.9186	0.0013	-89.1	1.3	680	15
BB2	72 44.94	66 59.69	1772	-0.23	-0.31	34.49	27.71	819	120	2285	2256	-0.36	236338	0.9234	0.0011	-84.3	1.1	640	15
BB2	72 44.94	66 59.69	1576	-0.03	-0.10	34.49	27.70	791	127	2298	2258	-0.30	236339	0.9279	0.0012	-79.9	1.2	600	15
BB2	72 44.94	66 59.69	1380	0.36	0.27	34.49	27.68	735	148	2284	2239	-0.25	236340	0.9432	0.0013	-64.6	1.3	470	15
BB2	72 44.94	66 59.69	1183	0.71	0.65	34.49	27.66	671	175	2285	2209	-0.16	236341	0.9726	0.0012	-35.4	1.2	225	15
BB2	72 44.94	66 59.69	986	1.18	1.13	34.51	27.64	651	188	2285	2212	-0.17	236342	0.9892	0.0013	-19.0	1.3	85	15
BB2	72 45.03	66 59.69	789	1.74	1.69	34.53	27.62	621	206	2284	2208	-0.09	236324	1.0142	0.0014	5.7	1.4	Modern	
BB2	72 45.03	66 59.69	592	1.41	1.36	34.43	27.56	578	215	2274	2205	-0.03	236325	1.0291	0.0014	20.6	1.4	Modern	
BB2	72 45.03	66 59.69	394	1.40	1.38	34.36	27.51	599	199	2270	2199	-0.13	236326	1.0281	0.0013	19.6	1.3	Modern	
BB2	72 45.03	66 59.69	197	0.19	0.37	34.00	27.29	519	236	2268	2157	-0.01	236327	1.0295	0.0014	21.0	1.4	Modern	
BB2	72 45.03	66 59.69	98	-1.37	-1.39	33.42	26.89	365	286	2242	2147	0.26	236328	1.0295	0.0013	20.9	1.3	Modern	
BB2	72 45.03	66 59.69	48	-1.68	-1.68	33.04	26.58	293	303	2249	2164	0.24	236329	1.0184	0.0015	10.0	1.5	Modern	
BB2	72 45.03	66 59.69	19	-0.92	-0.47	31.94	25.67	7	385	2228	2098	0.92	236330	1.0142	0.0013	5.8	1.3	Modern	
BB2†	72 45.03	66 59.69	3	2.23	NaN	29.81	23.80	0	336	2069	1937	1.14	236331	1.0153	0.0015	6.8	1.5	Modern	
													236332	1.0130	0.0014	4.6	1.4	Modern	
204†	73 16.11	57 59.97	789	1.27	1.24	34.50	27.63	0	198	2259	2201	-0.15	237455	1.0058	0.0015	-2.5	1.5	Modern	
													237456	1.0032	0.0016	-5.1	1.6	Modern	
204	73 16.11	57 59.97	592	1.49	1.46	34.49	27.60	0	204	2270	2204	-0.04	237457	1.0161	0.0017	7.7	1.7	Modern	
204	73 16.11	57 59.97	396	1.55	1.53	34.40	27.53	282	210	2263	2194	-0.01	237458	1.0180	0.0015	9.6	1.5	Modern	
204	73 16.11	57 59.97	196	0.74	0.71	34.03	27.28	428	233	2258	2180	-0.09	237459	1.0268	0.0015	18.2	1.5	Modern	
204	73 16.11	57 59.97	98	-0.46	-0.47	33.69	27.07	508	264	2233	2179	0.14	237460	1.0301	0.0015	21.6	1.5	Modern	
204	73 16.11	57 59.97	45	-0.84	-0.85	33.39	26.84	597	291	2240	2139	0.37	237461	1.0255	0.0015	17.0	1.5	Modern	
204†	73 16.11	57 59.97	18	2.77	2.65	32.81	26.15	609	364	2193	1996	1.73	237462	1.0238	0.0014	15.3	1.4	Modern	
													237463	1.0230	0.0014	14.5	1.4	Modern	
204	73 16.11	57 59.97	4	7.30	7.69	32.17	25.15	629	298	2180	2001	1.35	237464	1.0227	0.0015	14.2	1.5	Modern	
210†	75 25.16	61 33.60	1063	1.33	1.27	34.51	27.63	645	188	2327	2214	-0.19	237446	1.0021	0.0015	-6.2	1.5	Modern	
													237447	1.0036	0.0014	-4.8	1.4	Modern	
210	75 25.16	61 33.60	789	1.46	1.42	34.52	27.63	652	188	2273	2213	-0.12	237448	1.0028	0.0015	-5.5	1.5	Modern	
210	75 25.16	61 33.60	591	1.73	1.71	34.52	27.61	643	193	2291	2209	-0.10	237449	1.0073	0.0015	-1.1	1.5	Modern	
210	75 25.16	61 33.60	394	1.85	1.83	34.42	27.52	626	202	2272	2200	-0.16	237450	1.0178	0.0015	9.3	1.5	Modern	
210	75 25.16	61 33.60	197	0.41	0.32	33.98	27.26	518	236	2255	2176	-0.06	237451	1.0285	0.0016	20.0	1.6	Modern	
210	75 25.16	61 33.60	98	-0.46	-0.43	33.68	27.06	431	259	2250	2156	0.11	237454	1.0238	0.0016	15.3	1.6	Modern	

210	75 25.16	61 33.60	48	-0.90	-0.94	33.45	26.90	372	277	2241	2138	0.20	237443	1.0260	0.0015	17.5	1.5	Modern
210	75 25.16	61 33.60	18	0.01	0.32	33.13	26.60	0	384	2247	2060	1.11	237444	1.0253	0.0015	16.8	1.5	Modern
210	75 25.16	61 33.60	3	9.47	9.34	32.94	25.43	0	279	2218	2034	1.52	237445	1.0244	0.0015	15.9	1.5	Modern
108†	76 15.47	74 35.95	436	-0.06	-0.08	34.34	27.57	468	256	2295	2176	0.07	236343	1.0388	0.0014	30.1	1.4	Modern
													236344	1.0380	0.0014	29.4	1.4	Modern
108	76 15.47	74 35.95	256	-0.07	-0.07	34.25	27.50	473	255	2280	2178	-0.10	236345	1.0368	0.0013	28.2	1.3	Modern
108	76 15.47	74 35.95	226	-0.41	-0.42	33.94	27.27	461	258	2262	2159	-0.11	236346	1.0329	0.0013	24.3	1.3	Modern
108	76 15.47	74 35.95	137	-1.28	-1.29	32.92	26.49	286	308	2245	2144	0.24	236347	1.0121	0.0013	3.7	1.3	Modern
108	76 15.47	74 35.95	39	-1.53	-1.55	32.36	26.01	232	324	2242	2133	0.22	236348	1.0147	0.0014	6.3	1.4	Modern
108	76 15.47	74 35.95	18	1.76	1.37	31.58	25.45	1	357	2195	2017	1.17	236349	1.0078	0.0013	-0.6	1.3	Modern
108	76 15.47	74 35.95	4	3.12	NaN	31.14	NaN	0	348	2158	1979	1.42	236350	1.0029	0.0016	-5.4	1.6	Modern
323	74 09.57	80 28.23	740	0.59	0.56	34.46	27.64	574	207	2282	2137	0.00	240002	1.0161	0.0016	7.7	1.6	Modern
323	74 09.57	80 28.23	592	0.86	0.80	34.46	27.62	578	217	2279	2203	-0.09	239998	1.0181	0.0016	9.6	1.6	Modern
323	74 09.57	80 28.23	394	0.87	0.81	34.35	27.53	550	228	2275	2190	-0.08	239999	1.0315	0.0016	22.9	1.6	Modern
323	74 09.57	80 28.23	196	-1.06	-1.05	33.75	27.14	436	272	2262	2178	0.07	240000	1.0260	0.0016	17.5	1.6	Modern
323	74 09.57	80 28.23	98	-1.34	-1.33	32.91	26.47	400	289	2240	2157	0.18	240001	1.0203	0.0015	11.8	1.5	Modern
323	74 09.57	80 28.23	48	-1.66	-1.66	32.57	26.20	308	315	2244	2171	0.37	240003	1.0067	0.0017	-1.7	1.7	Modern
323†	74 09.57	80 28.23	19	-1.01	-0.97	32.16	25.85	32	384	2207	2040	0.71	240007	1.0109	0.0016	2.5	1.6	Modern
													240008	1.0077	0.0017	-0.6	1.7	Modern

Table A2: Modeled anthropogenic carbon (C_{anth}) concentrations calculated from the ΔC^* proxy based on calculations presented by Lee et al., (2003). Bomb $\Delta^{14}C$ and Natural (measured – bomb) $\Delta^{14}C$ signatures presented calculated from the potential alkalinity (Palk) method presented by Rubin and Key., (2002).

Station	Latitude (°N)	Longitude (°W)	Depth (m)	DIC_{anth} (µmol/kg)	$\Delta^{14}C_{canth}$ (‰)	$\Delta^{14}C_{bomb}$ (‰)	$\Delta^{14}C_{natural}$ (‰)
193	66 46.18	59 20.41	787	0.0	-7.9	46.6	-54.6
193	66 46.18	59 20.41	592	15.9	12.4	45.9	-33.6
193	66 46.18	59 20.41	393	25.4	28.8	68.4	-39.6
193	66 46.18	59 20.41	196	40.0	36.5	64.7	-28.2
193	66 46.18	59 20.41	98	9.7	25.2	85.0	-59.8
193	66 46.18	59 20.41	48	0.0	16.0	109.6	-93.6
193	66 46.18	59 20.41	18	0.0	15.7	88.5	-72.8
193	66 46.18	59 20.41	3	0.0	7.6	158.5	-150.9
196	66 59.21	56 03.57	97	19.7	30.0	73.1	-43.1
196	66 59.21	56 03.57	48	24.4	28.9	72.9	-44.0
196	66 59.21	56 03.57	18	22.8	34.2	80.5	-46.3
196	66 59.21	56 03.57	4	32.9	35.9	47.3	-11.3
BB15	68 27.08	55 53.99	394	18.5	24.9	92.5	-67.6
BB15	68 27.08	55 53.99	197	18.4	27.9	88.5	-60.6
BB15	68 27.08	55 53.99	98	11.0	22.4	81.8	-59.4
BB15	68 27.08	55 53.99	48	0.0	19.4	93.6	-74.2
BB15	68 27.08	55 53.99	18	0.0	18.5	104.4	-85.9
BB15	68 27.08	55 53.99	3	0.0	15.9	98.4	-82.4
BB18	70 05.40	52 44.40	396	6.4	19.2	93.2	-74.1
BB18	70 05.40	52 44.40	196	11.9	22.5	90.2	-67.7
BB18	70 05.40	52 44.40	98	0.0	17.6	85.5	-67.9
BB18	70 05.40	52 44.40	48	0.0	21.6	97.1	-75.5
BB18	70 05.40	52 44.40	19	0.0	19.6	101.0	-81.4
BB18	70 05.40	52 44.40	3	0.0	18.1	103.3	-85.2
227	70 47.81	56 59.27	394	6.0	17.2	76.3	-59.1
227	70 47.81	56 59.27	197	16.8	26.8	58.3	-31.5
227	70 47.81	56 59.27	98	7.0	21.0	82.7	-61.7
227	70 47.81	56 59.27	48	0.0	20.8	90.1	-69.4
227	70 47.81	56 59.27	19	34.5	36.0	87.9	-51.9
227	70 47.81	56 59.27	4	0.0	20.2	142.4	-122.2
224	70 25.20	62 56.71	1969	0.0	-89.5	0.0	-89.5
224	70 25.20	−62 56.71	1773	0.0	-86.7	0.0	-86.7
224	70 25.20	−62 56.71	1576	0.0	-82.0	0.0	-82.0
224	70 25.20	−62 56.71	1380	0.0	-73.4	0.0	-73.4
224	70 25.20	−62 56.71	1183	0.0	-52.6	10.1	-62.7
224	70 25.20	−62 56.71	986	0.0	-22.3	34.6	-56.8
224	70 26.44	−62 58.89	789	5.6	-2.8	49.1	-52.0

224	70 26.44	−62 58.89	592	7.5	10.9	68.6	-57.7
224	70 26.44	−62 58.89	394	9.6	24.1	82.5	-58.4
224	70 26.44	−62 58.89	197	0.0	18.1	92.6	-74.5
224	70 26.44	−62 58.89	98	0.0	15.3	126.2	-110.9
224	70 26.44	−62 58.89	48	16.4	15.8	127.1	-111.3
224	70 26.44	−62 58.89	19	31.7	22.9	152.8	-129.9
224	70 26.44	−62 58.89	3	0.0	8.7	204.3	-195.6
BB2	72 44.94	66 59.69	2262	0.0	-90.0	0.0	-90.0
BB2	72 44.94	66 59.69	1968	0.0	-89.1	0.0	-89.1
BB2	72 44.94	66 59.69	1772	0.0	-84.3	0.0	-84.3
BB2	72 44.94	66 59.69	1576	0.0	-79.9	1.9	-81.8
BB2	72 44.94	66 59.69	1380	0.0	-64.6	1.5	-66.1
BB2	72 44.94	66 59.69	1183	0.0	-35.4	30.3	-65.7
BB2	72 44.94	66 59.69	986	0.0	-19.0	45.2	-64.2
BB2	72 45.03	66 59.69	789	11.2	10.9	66.5	-55.6
BB2	72 45.03	66 59.69	592	13.7	27.0	77.1	-50.2
BB2	72 45.03	66 59.69	394	0.0	19.6	77.4	-57.8
BB2	72 45.03	66 59.69	197	0.0	21.0	98.3	-77.4
BB2	72 45.03	66 59.69	98	0.0	20.9	107.1	-86.2
BB2	72 45.03	66 59.69	48	14.9	17.0	127.2	-110.2
BB2	72 45.03	66 59.69	19	41.7	26.2	172.2	-146.0
BB2	72 45.03	66 59.69	3	0.0	5.7	160.7	-155.0
204	73 16.11	57 59.97	789	0.0	-3.8	35.2	-39.1
204	73 16.11	57 59.97	592	8.5	11.6	57.6	-46.0
204	73 16.11	57 59.97	396	8.1	13.3	57.4	-44.1
204	73 16.11	57 59.97	196	0.0	18.2	83.0	-64.7
204	73 16.11	57 59.97	98	21.0	31.5	82.4	-50.9
204	73 16.11	57 59.97	45	0.0	17.0	100.4	-83.4
204	73 16.11	57 59.97	18	0.0	14.9	82.9	-68.0
204	73 16.11	57 59.97	4	28.6	28.9	113.2	-84.3
210	75 25.16	61 33.60	1063	0.0	-5.5	99.2	-104.7
210	75 25.16	61 33.60	789	0.0	-5.5	46.4	-52.0
210	75 25.16	61 33.60	591	0.0	-1.1	67.9	-69.0
210	75 25.16	61 33.60	394	7.8	12.9	65.6	-52.7
210	75 25.16	61 33.60	197	0.0	20.0	85.1	-65.1
210	75 25.16	61 33.60	98	0.0	15.3	93.4	-78.1
210	75 25.16	61 33.60	48	0.0	17.5	100.4	-82.9
210	75 25.16	61 33.60	18	0.0	16.8	117.8	-101.0
210	75 25.16	61 33.60	3	45.9	39.3	100.6	-61.2
108	76 15.47	74 35.95	436	0.0	29.8	109.9	-80.1
108	76 15.47	74 35.95	256	0.0	28.2	99.4	-71.2
108	76 15.47	74 35.95	226	0.0	24.3	97.8	-73.5
108	76 15.47	74 35.95	137	9.4	8.2	125.8	-117.7
108	76 15.47	74 35.95	39	14.0	12.9	162.1	-149.1
108	76 15.47	74 35.95	18	0.0	-0.6	157.1	-157.6
108	76 15.47	74 35.95	4	0.0	-5.4	145.4	-150.8

323	74 09.57	80 28.23	740	0.0	7.7	70.1	-62.4
323	74 09.57	80 28.23	592	0.0	9.6	69.4	-59.8
323	74 09.57	80 28.23	394	0.0	22.9	84.7	-61.8
323	74 09.57	80 28.23	196	0.0	17.5	103.0	-85.5
323	74 09.57	80 28.23	98	13.1	18.0	131.2	-113.2
323	74 09.57	80 28.23	48	41.5	17.8	144.3	-126.5
323	74 09.57	80 28.23	19	0.0	1.0	129.8	-128.8

Appendix B: DIC $\delta^{13}C$ and $\Delta^{14}C$ least squares regression analysis and statistics summary

Table B1 – Potential density (kg m^{-3}) versus DIC $\delta^{13}C$ (‰) least squares linear regression statistics for slope coefficients, y-intercepts, coefficients of determination (R^2) and p-values

Station	Slope	±Slope Error	y-intercept	±y-intercept error	R^2	p-value
193	-0.42	0.13	11.6	3.6	0.617	0.047
196	-1.47	0.22	40.1	5.9	0.957	0.045
BB15	-1.57	0.22	42.7	6.0	0.925	0.005
BB18	-0.80	0.07	21.4	6.0	0.971	0.002
227	-1.52	0.12	41.5	3.2	0.976	0.001
224	-0.32	0.05	8.5	1.5	0.743	<0.001
BB2	-0.39	0.03	10.7	0.9	0.919	<0.001
204	-0.74	0.16	20.3	4.3	0.782	0.011
210	-0.82	0.11	22.5	2.9	0.895	<0.001
108	-0.53	0.10	14.4	2.6	0.851	0.005
323	-0.44	0.04	11.9	1.0	0.958	<0.001

Table B2 – Potential density (kg m^{-3}) versus DIC $\Delta^{14}C$ (‰) least squares linear regression statistics for slope coefficients, y-intercepts, coefficients of determination (R^2) and p-values.

Station	Slope	±Slope Error	y-intercept	±y-intercept error	R^2	p-value
193	-0.73	3.45	30.9	92.7	0.007	0.483
196	-1.62	9.15	63.3	245.5	0.015	0.820
BB15	0.34	1.70	8.6	45.9	0.010	0.374
BB18	-0.49	0.92	31.3	24.5	0.066	0.936
227	-2.53	1.70	86.7	45.9	0.357	0.674
224	-18.90	10.18	488.4	275.8	0.223	0.124
BB2	-17.35	10.60	447.0	287.7	0.171	0.170
204	-3.55	3.48	107.9	93.6	0.148	0.667
210	-8.74	4.37	245.7	118.3	0.364	0.156
108	13.00	1.80	-331.4	47.7	0.912	0.005
323	7.56	3.98	-193.6	107.2	0.419	0.072

Table B3 – Salinity versus DIC $\delta^{13}C$ (‰) least squares linear regression statistics for slope coefficients, y-intercepts, coefficients of determination (R^2) and p-values.

Station	Depth	Slope	±Slope Error	y-intercept	±y-intercept error	R^2	p-value
193	Surface	-0.18	0.27	6.7	8.7	0.190	0.564
	Mid-Depth	1.63	0.39	-56.2	13.5	0.896	0.053
196	Surface	-2.30	0.60	77.8	20.3	0.879	0.063
BB15	Surface	-3.87	1.27	131.0	42.8	0.822	0.093
BB18	Surface	-0.83	0.14	27.9	4.6	0.946	0.027
227	Surface	-3.43	0.70	116.1	23.5	0.923	0.039
224	Surface	-0.11	0.02	3.9	0.7	0.928	0.037
	Mid-Depth	-0.05	0.04	1.6	1.3	0.480	0.307
	Deep-Depth	-22.58	29.70	778.5	1024.3	0.126	0.489
BB2	Surface	-0.25	0.09	8.8	2.9	0.800	0.106
	Mid-Depth	-0.13	0.15	4.5	5.1	0.290	0.461
	Deep-Depth	6.28	3.48	-217.0	120.1	0.395	0.131
204	Surface	-0.90	0.50	30.7	16.4	0.622	0.211
	Mid-Depth	0.01	0.20	-0.3	7.0	0.001	0.974
210	Surface	-2.03	0.34	68.2	11.3	0.947	0.027
	Mid-Depth	-0.15	0.10	5.0	3.3	0.441	0.222
108	Surface	-0.99	0.34	32.3	10.9	0.893	0.212
	Mid-Depth	-0.19	0.12	6.5	4.0	0.569	0.246
323	Surface	-0.40	0.06	13.5	1.9	0.959	0.021
	Mid-Depth	-0.17	0.09	5.9	3.2	0.625	0.209

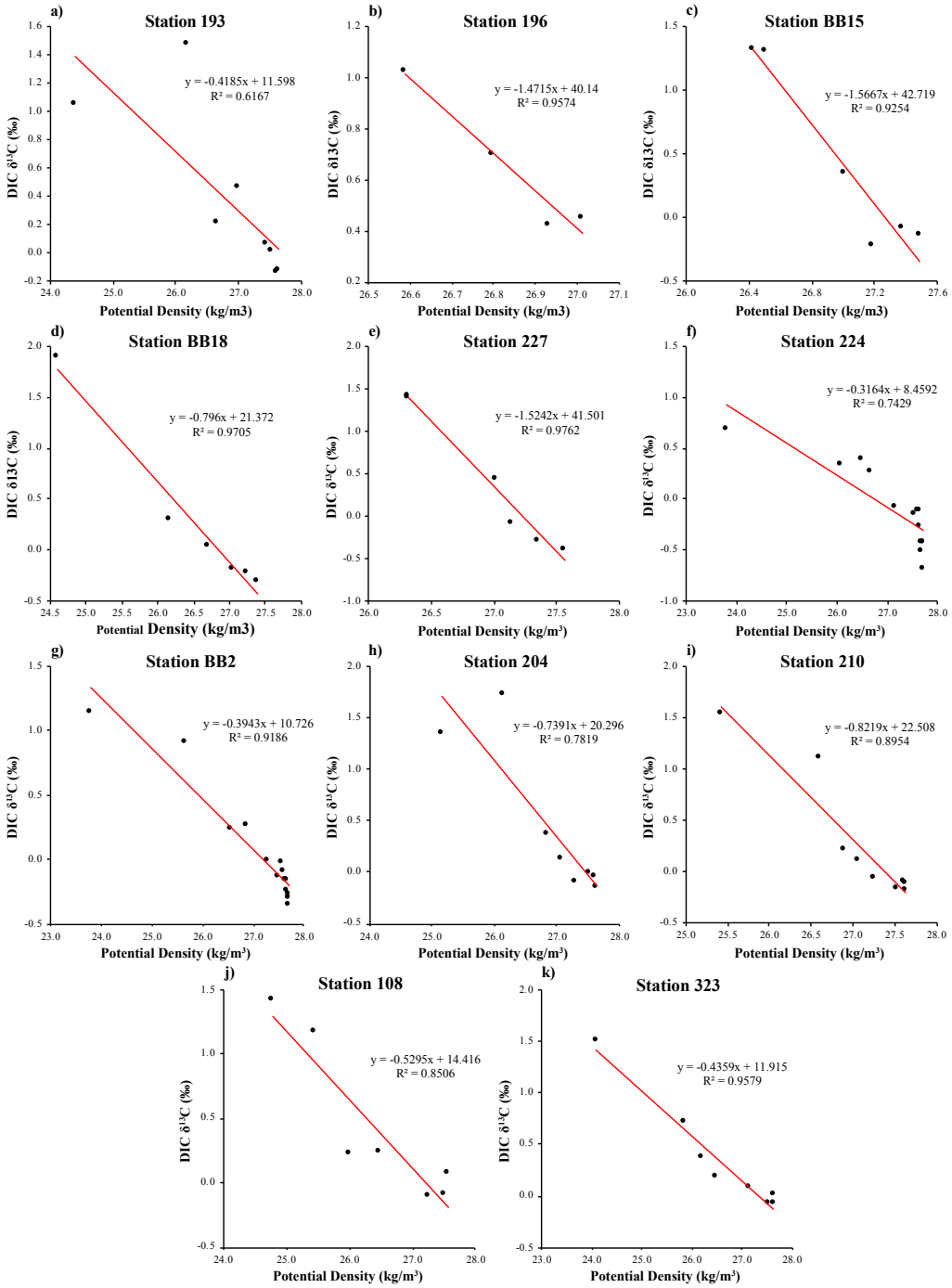

Figure B1 – Regressions of potential density versus DIC $\delta^{13}C$ for Baffin Bay stations. Lines are Least squares fit linear regression. Line equations and coefficients of determination (R^2) values are listed next to the trendline.

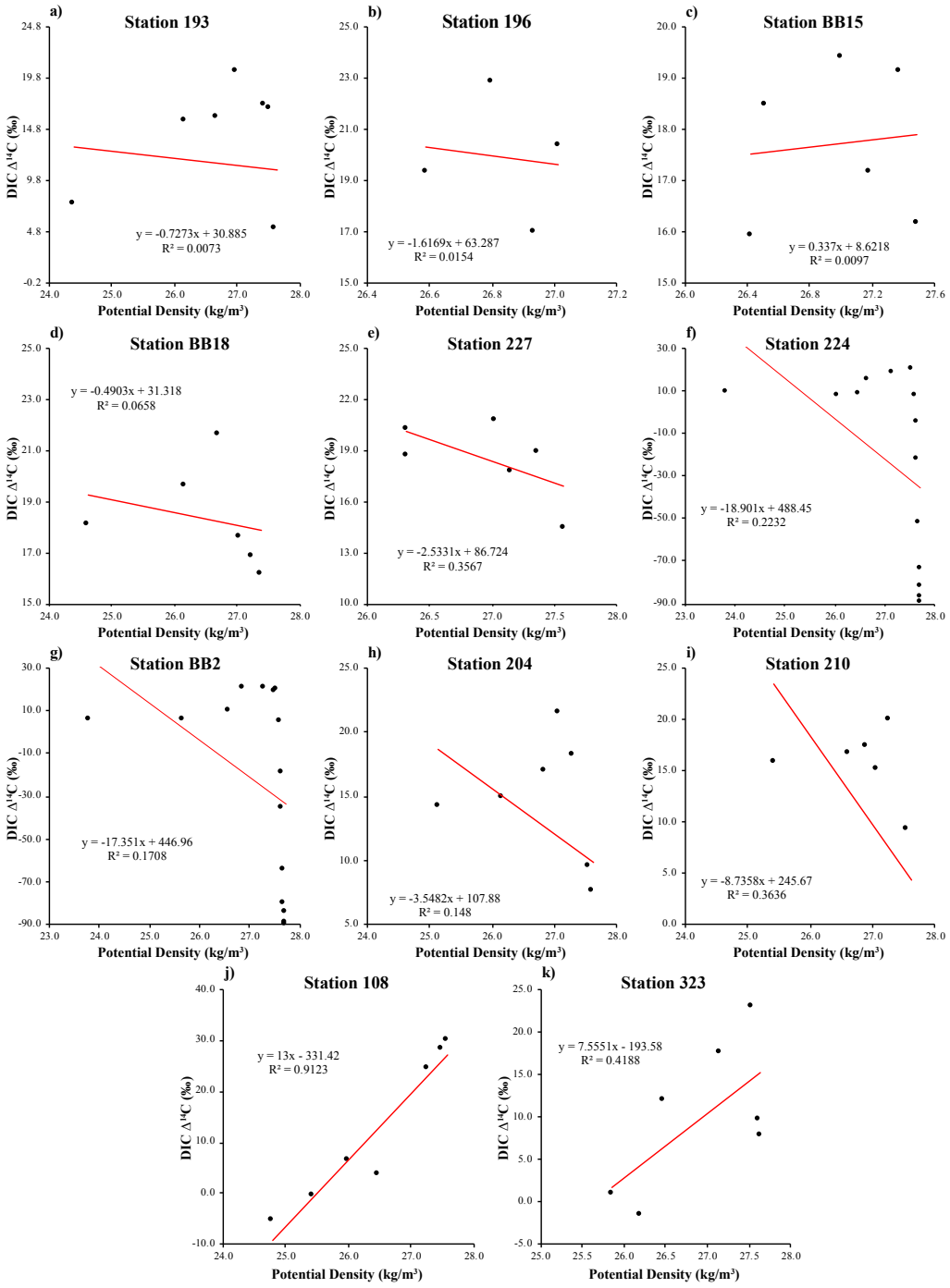

Figure B2 – Regressions of potential density versus DIC $\Delta^{14}C$ for Baffin Bay stations. Lines are Least squares fit linear regression. Line equations and coefficients of determination (R^2) values are listed next to the trendline.

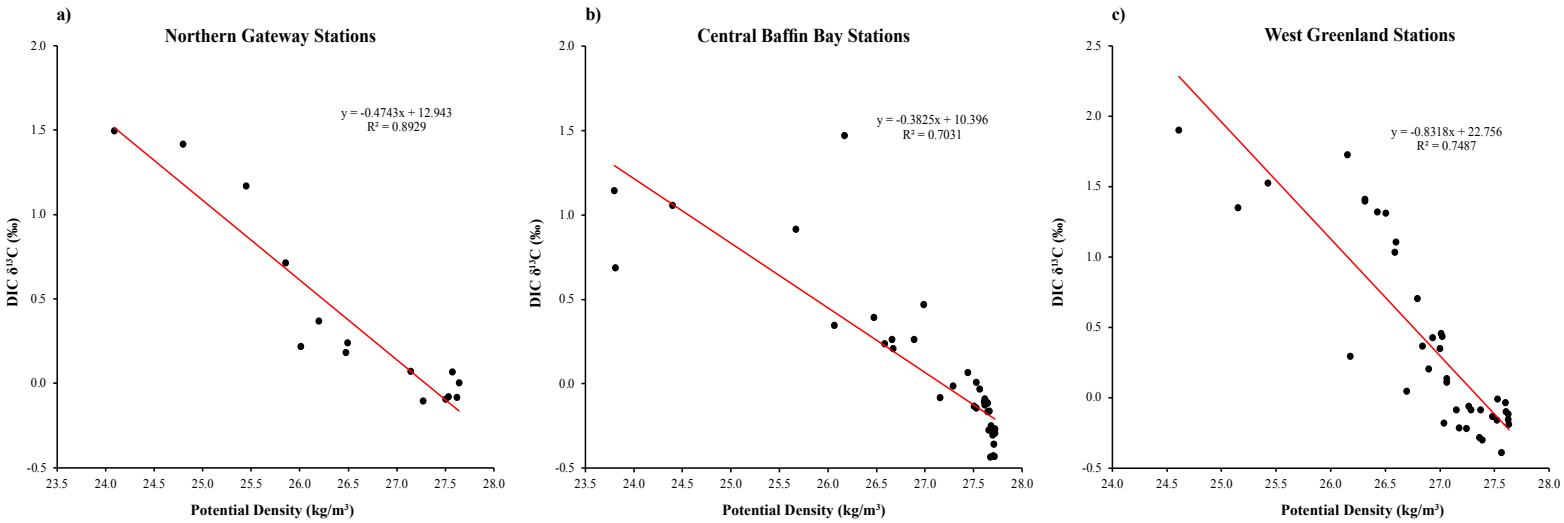

Figure B3 – Regressions of potential density versus DIC $\delta^{13}C$ for distinct regions in Baffin Bay; Northern Gateway stations consist of 108 and 323, Central Baffin Bay stations consist of 193, BB2, and 224, and West Greenland stations consist of 196, BB15, BB18, 227, 204, and 210. Lines are Least squares fit linear regression. Line equations and coefficients of determination (R^2) values are listed next to the trendline.

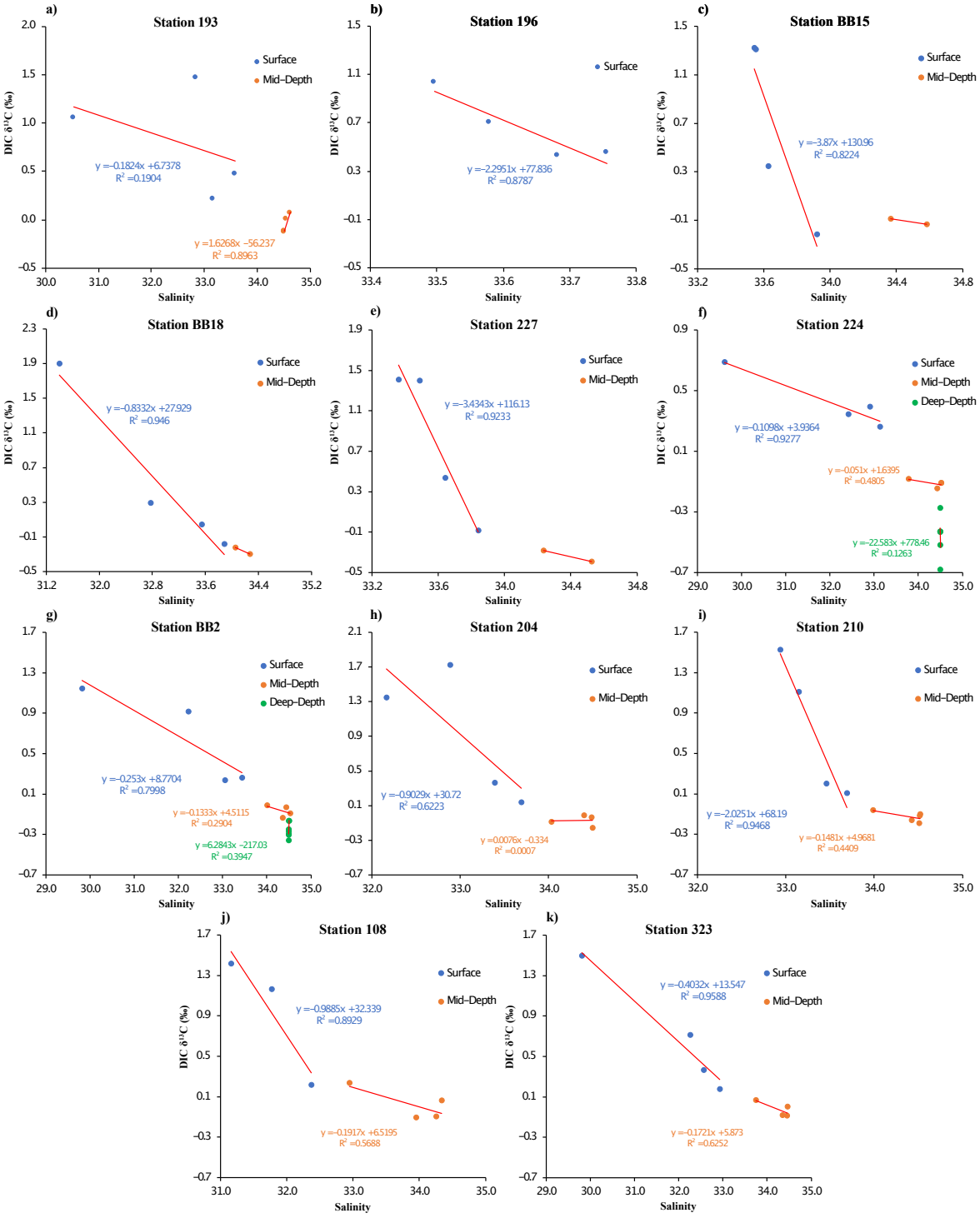

Figure S4 – Regressions of salinity versus DIC $\delta^{13}C$ for Baffin Bay stations for surface, mid-depth and deep sample data. Depth-specific regressions are shown for; surface (0 – 100m), mid-depth (100 – 800m), and deep (>800m). Lines are Least squares fit linear regression. Line equations and coefficients of determination (R^2) values are listed next to each trendline.